DISEASES AND DISORDERS

Environmental eustress improves postinfarction cardiac repair via enhancing cardiac macrophage survival

Pei-Yuan Bai[1,2,3]†, Si-Qin Chen[2,3,4]†, Dai-Le Jia[1,2,3]†, Li-Hong Pan[2,3,4]†, Chao-Bao Liu[5], Jin Liu[1,2,3], Wei Luo[1,2,3], Yang Yang[6], Ma-Yu Sun[6], Nai-Fu Wan[7], Wu-Wei Rong[7], Ai-Jun Sun[1,2,3,4]*, Jun-Bo Ge[1,2,3,4]

Macrophages play a vital role in cardiac repair following myocardial infarction (MI). An enriched environment (EE) is involved in the regulation of macrophage-related activities and disease progression; however, whether EE affects the phenotype and function of macrophages to improve postinfarction cardiac repair remains unknown. In this study, we found that EE improved cardiac function, decreased mortality, and ameliorated adverse ventricular remodeling in mice after MI, with these outcomes closely related to the increased survival of Ly6C^{low} macrophages and their CCR2^{-}MHCII^{low} subsets. EE increased the expression of brain-derived neurotrophic factor (BDNF) in the hypothalamus, leading to higher circulating levels of BDNF, which, in turn, regulated the cardiac macrophages. BDNF bound to tropomyosin receptor kinase B to activate downstream ERK1/2 and AKT pathways, promoting macrophage survival. These findings demonstrate that EE optimizes postinfarction cardiac repair and highlights the significance of EE as a previously unidentified strategy for impeding adverse ventricular remodeling.

INTRODUCTION

Acute myocardial infarction (MI) is a common and life-threatening coronary heart disease (CHD). Despite current treatments, mortality and heart failure caused by MI remain substantial (*1*). Psychosocial stress is critically involved in the initiation and progression of MI (*2*). Numerous studies have highlighted the deleterious effects of "distress" (negative stress) on CHD. The INTERHEART study on a cohort of 25,000 individuals in 52 countries found that people with chronic stress at work or home had >2.1 times the risk of developing an MI than their counterparts (*3*); however, whether eustress (positive stress) (*4*) exerts a cardioprotective role in the context of MI has not been clarified. Here, we examined the effect of eustress on cardiac repair following MI.

Living in an enriched environment (EE) with increased dynamic social interactions, frequent exposure to novel objects, and enhanced physical activity has been established as a model of eustress (*5*, *6*). Apart from its neurobiological and behavioral effects, multiple lines of evidence illustrate that EE affects inflammation and the immune response. For example, EE inhibits the adiponectin-mediated activation of intracranial macrophages and microglia and has notable therapeutic effects on corticosterone-induced depression in mice (*7*). In addition, Bacillus Calmette-Guérin vaccination combined with EE promotes neurogenesis and spatial cognition by changing the M2 polarization of meningeal macrophages (*8*). These studies suggest that the mechanisms through which EE improves disease outcomes at least partially involve its regulatory effects on macrophages (*9*, *10*). Moreover, previous studies extrapolated research findings regarding the effect of EE on learning and memory to its effects on common maladies, such as ischemic brain injury, neurodegenerative disorders, and cancer (*11*, *12*). Recently, the benefits of EE were linked to the amelioration of cardiovascular diseases, such as hypertension and atherosclerosis (*13*, *14*). However, the role of EE in MI remains unknown.

Inflammation is required for cardiac repair and wound healing following MI (*15*, *16*), and immune cells are involved in MI occurrence and development (*17*). A clinical trial showed that canakinumab, a human monoclonal antibody against interleukin-1β, significantly reduced the recurrence rate of cardiovascular events (*18*). Cardiac repair includes three overlapping phases—acute inflammation, fiber proliferation, and stable maturity—each closely linked to inflammation. During post-MI repair, the transition of macrophages from a proinflammatory to proresolving state promotes extracellular matrix (ECM) synthesis and angiogenesis (*19*). Because excessive or insufficient inflammation is inconducive to cardiac healing, precise regulation of immune inflammation is essential for post-MI repair (*20*). We hypothesized that EE may also participate in post-MI cardiac repair by targeting immune inflammation.

In this study, we used flow cytometry and mice harboring multiple reporter genes and brain-specific brain-derived neurotrophic factor (BDNF) knockdown to find an intriguing mechanism underlying the cardioprotective effect of EE involving a brain–cardiac macrophage axis mediated by BDNF. Collectively, these data underscore the potential for environmental eustress via EE to provide an innovative strategy for impeding adverse cardiac remodeling post-MI.

RESULTS

Study design and establishment of the EE model

Mice (3 to 4 weeks old) were housed under standard environment (SE) or EE conditions for 4 weeks, followed by the performance of a permanent left anterior descending (LAD)–artery ligation (Fig. 1A). The SE setup was 26 cm by 16 cm by 13 cm without any supplements, and the EE was 61 cm by 43 cm by 21 cm supplemented with

[1]Department of Cardiology, Zhongshan Hospital, Fudan University, Shanghai Institute of Cardiovascular Diseases, Shanghai, China. [2]Key Laboratory of Viral Heart Diseases, National Health Commission, Shanghai, China. [3]Key Laboratory of Viral Heart Diseases, Chinese Academy of Medical Sciences, Shanghai, China. [4]Institutes of Biomedical Sciences, Fudan University, Shanghai, China. [5]School of Basic Medical Sciences, Fudan University, Shanghai, China. [6]State Key Laboratory of Oncogenes and Related Genes, Center for Single-Cell Omics, School of Public Health, Shanghai Jiao Tong University School of Medicine, Shanghai, China. [7]Department of Cardiology, Ruijin Hospital, Shanghai Jiaotong University School of Medicine, Shanghai, China.
*Corresponding author. Email: sun.aijun@zs-hospital.sh.cn
†These authors contributed equally to this work.

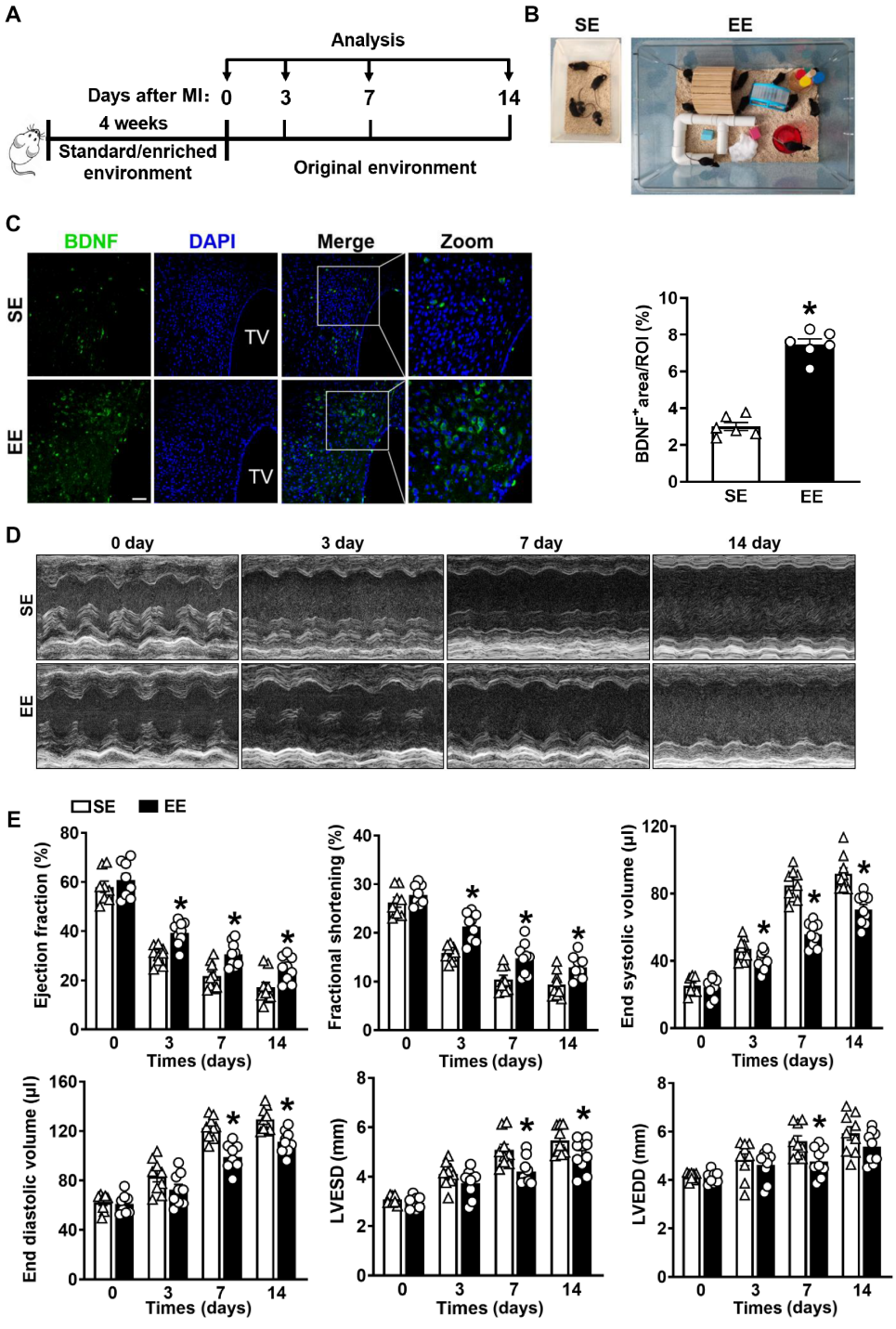

Fig. 1. Model establishment and cardiac function comparison between SE and EE mice after MI. (**A**) Timeline diagram of the experimental procedures. (**B**) Cage setup of the SE and EE housing. (**C**) Immunostaining analyses of BDNF in the hypothalamus of wild-type (WT) mice after 4 weeks of SE and EE housing ($n = 6$). TV, third ventricle; *$P < 0.05$ versus SE mice. Scale bars, 40 μm. DAPI, 4′,6-diamidino-2-phenylindole. (**D**) Typical M-mode images of the hearts were obtained from mice at days 3, 7, and 14 after MI or sham surgery. (**E**) EF, FS, left ventricular ESV, left ventricular EDV, LVESD, and LVEDD were measured using echocardiography at 3, 7, and 14 days after MI or sham surgery ($n = 8$ to 9). *$P < 0.05$ versus SE. Data are expressed as means ± SEM. Data in (C) were analyzed using the Student's *t* test. Data in (E) were analyzed using two-way analysis of variance (ANOVA) followed by Bonferroni post hoc analysis.

running wheels, tunnels, wooden toys, small huts, and nesting materials. The EE housing contained more mice, and the elements were regularly changed (Fig. 1B and movies S1 and S2). Previous studies demonstrated that an increased expression of BDNF in the hypothalamus can confirm the success of EE induction (*21*). In the present study, immunostaining confirmed significantly higher BDNF expression in the hypothalamus of EE mice relative to SE mice (Fig. 1C). Moreover, Western blotting, quantitative polymerase chain reaction (qPCR), and immunohistochemical assays confirmed markedly elevated BDNF expression in the hypothalamus of EE mice compared with that in SE mice (fig. S1, A to C). Collectively, these findings demonstrate the successful establishment of the EE mouse model.

EE ameliorates myocardial dysfunction, improves long-term survival, and limits adverse remodeling after MI

We first examined the effect of EE housing on cardiac function. At baseline, the cardiac function in EE mice was comparable to that in SE mice (table S1). Echocardiographic parameters, including left ventricular ejection fraction (LVEF), fractional shortening (FS), end-systolic volume (ESV), and left ventricular end-systolic dimension (LVESD), were significantly improved in EE mice compared with those in SE controls on days 3, 7, and 14 after MI (Fig. 1, D and E, and fig. S2A). In addition, left ventricular chamber dilation was alleviated in EE mice, as evidenced by a marked decrease in end-diastolic volume (EDV), ESV, left ventricular end-diastolic dimension (LVEDD), and LVESD (Fig. 1, D and E, and fig. S2A). Furthermore, the heart weight–to–body weight ratio and lung weight–to–body weight ratio in EE mice were significantly lower than those in SE controls, suggesting attenuation of pulmonary edema and congestive heart failure in EE mice after MI (fig. S2B).

Compared with SE controls, EE housing robustly improved post-MI survival, as 52% of SE-housed mice survived 4 weeks after MI, consistent with data reported by other studies, whereas the survival rate of EE mice increased to 72% (Fig. 2A). In addition, hematoxylin and eosin (H&E) staining showed significantly ameliorated ventricular remodeling 14 days after MI in EE mice compared with SE mice, as illustrated by a decreased infarct size and increased wall thickness at the infarct site (Fig. 2B). To further elucidate the mechanisms underlying the attenuated cardiac remodeling in EE mice, we assessed the collagen volume fraction in the infarct area. Masson's trichrome staining (TC) and Picrosirius red staining of cardiac transverse sections at the papillary level revealed that collagen density in the infarct area was significantly greater in EE hearts than in SE hearts 14 days after MI (Fig. 2, C and D). However, the collagen density in the noninfarct area was comparable between EE and SE mice (Fig. 2E). Collectively, our data confirm the beneficial effects of EE on post-MI wound healing.

EE mitigates the inflammatory response and cardiomyocyte apoptosis after MI

Previous studies have shown that both the inflammatory response and cardiomyocyte apoptosis are closely related to cardiac remodeling (*22*). In the present study, the results demonstrated that the EE infarcts exhibited a lower inflammatory transcriptional signature than SE infarcts, as evidenced by the down-regulation of major proinflammatory genes, such as *Il1b*, *Il6*, tumor necrosis factor–α (*Tnfa*), inducible nitric oxide synthase, and matrix metallopeptidase 9, and up-regulation of major anti-inflammatory genes, including *Il10*, transforming growth factor–β1, and vascular endothelial growth factor (*Vegf*) (fig. S3, A and B), although some genes merely showed an upward or downward trend. Apoptosis and necrosis of cardiomyocytes caused by MI are important pathological features for adverse cardiac remodeling. Furthermore, terminal deoxynucleotidyl transferase–mediated deoxyuridine triphosphate nick end labeling (TUNEL) staining to detect cardiomyocyte apoptosis at days 7 and 14 after MI revealed a significant reduction in TUNEL-positive cardiomyocytes in EE mice relative to those in SE controls (fig. S3C), which agreed with the findings that EE can reduce inflammation and improve ventricular remodeling after MI.

EE enhances ECM synthesis and increases the number of Ly6C^{low} macrophages

Damaged hearts initiate repair through a series of activities, including enhancement of ECM synthesis and activation of reparative macrophages 4 days after MI (*19*). Effective ECM formation in the infarct area is necessary for preventing heart rupture. Immunoblotting, immunostaining, and real-time PCR assays identified distinctly higher expression levels of α–smooth muscle actin (SMA), collagen I, and collagen III in the infarct area of EE mice relative to those in SE mice after MI (Fig. 3, A to C, and fig. S4, A to C). In addition, infarcts of SE- and EE-housed mice harbored a comparable number of F4/80$^+$ macrophages (fig. S5A); however, arginase-1 (Arg-1) M2-like reparative macrophages were more abundant in infarcts of EE-housed mice than in those of SE-housed controls at 7 and 14 days after MI (fig. S5B). Moreover, flow cytometric examination of the influence of EE on M1- and M2-like macrophages revealed a significant downward shift in the number of M1-like macrophages at different time points in EE mice than in SE mice after MI (fig. S5C). By contrast, M2-like macrophages exhibited an upward trend in EE-housed mice compared with SE-housed mice at 7 and 14 days after MI, although there were no differences 3 days after MI (fig. S5C).

In addition to the M1/M2 classification, we used Ly6C to identify two subsets of macrophages with distinct functions, namely, Ly6C^{high} and Ly6C^{low} macrophages. For this analysis, we isolated CD45$^+$CD11b$^+$Ly6G$^-$Ly6C$^+$ monocytes/macrophages (Mos/Mps) from the infarcted hearts of mice. Notably, we observed an increase in CD45$^+$CD11b$^+$Ly6G$^-$F4/80$^+$Ly6C^{low} Mps in EE mice compared with SE mice across all time points (Fig. 3D), although the total quantities of Mos/Mps were comparable between groups (fig. S5D). Furthermore, according to previous studies, Ly6C^{low} macrophages express high levels of CX3C chemokine receptor 1 (CX3CR1) (*23*, *24*); therefore, we used CX3CR1-GFP (green fluorescent protein) mice to visualize CX3CR1-expressing cells and further confirm the effect of EE on Ly6C^{low} macrophages in the infarct area. We observed a significantly higher number of CX3CR1-GFP$^+$ cells in EE-housed mice than in SE-housed mice (Fig. 3E). These data indicated that EE promoted more effective cardiac repair after MI, which agreed with the results showing that EE improved cardiac function and attenuated adverse remodeling.

In addition to assessing macrophages and their subsets, we also evaluated alterations in neutrophils or lymphocytes in infarct tissues, finding no significant changes in these cell components in either the EE- or SE-housed groups (fig. S6, A and B). Furthermore, we examined immune cell profiles in peripheral blood, bone marrow, and spleen at 7 and 14 days after MI. Although we identified variations in some immune cell populations, there were no significant differences between the EE- and SE-housed mice (figs. S7 to S9).

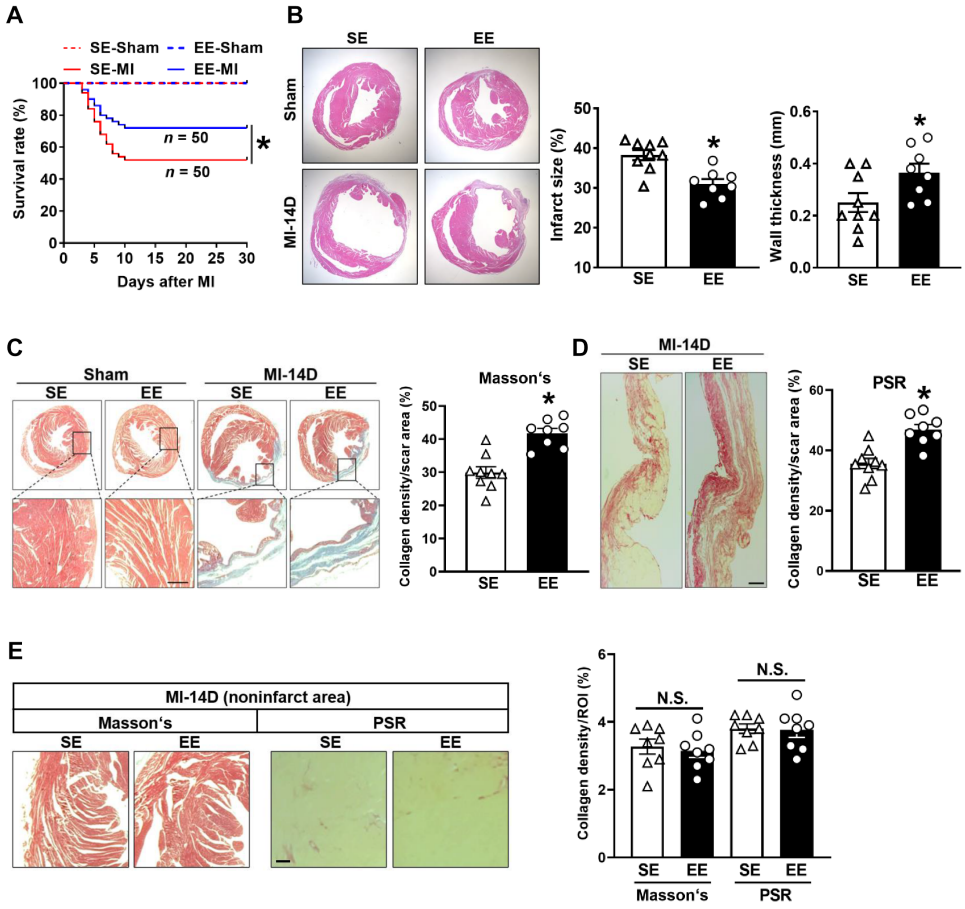

Fig. 2. Effects of EE on survival, infarct size, wall thickness, and myocardial fibrosis after MI. (**A**) Kaplan-Meier survival analysis at different time points after MI. *$P < 0.05$ versus SE MI. (**B**) Representative H&E staining of cardiac tissue obtained from SE and EE mice at day 14 after MI or sham operation. Quantitative analysis of the infarct size and wall thickness in MI group ($n = 9$ for SE and $n = 8$ for EE). *$P < 0.05$ versus SE. (**C**) Representative Masson's staining of cardiac tissue and enlarged view of the indicated region at 14 days after MI or sham surgery. Collagen density was measured as the total collagen area divided by scar area examined ($n = 9$ for SE and $n = 8$ for EE). *$P < 0.05$ versus SE. (**D**) Representative Picrosirius red (PSR) staining of SE and EE mice at day 14 after MI. Scale bar, 100 μm. Quantification of collagen density ($n = 9$ for SE and $n = 8$ for EE). *$P < 0.05$ versus SE. (**E**) Representative Masson's and PSR staining of the noninfarct area of SE- and EE-treated mice at day 14 after MI. Scale bar, 50 μm. Quantification of collagen density in the noninfarct area ($n = 8$). ROI, region of interest. N.S., no significance. Data are expressed as means ± SEM. Survival distributions were estimated using the Kaplan-Meier method and compared using the log-rank test. Data in (B to E) were analyzed using Student's *t* test.

EE promotes angiogenesis mediated by Ly6C^{low} macrophages

Myocardial angiogenesis plays a crucial role in wound healing and cardiac remodeling. Moreover, one of the critical mechanisms through which EE contributes to the recovery from various diseases involves the promotion of angiogenesis, an effect that has been demonstrated in cerebrovascular disease and optic nerve injury. Thus, we evaluated the effect of EE on angiogenesis. EE treatment significantly enhanced angiogenesis, as evidenced by an increase in CD31$^+$ endothelial cells in the infarct site (Fig. 4A). Accordingly, the labeling of CD31$^+$/proliferating cell nuclear antigen–positive (PCNA$^+$) cells in the ischemic zone showed that neovascularization in EE mice was significantly increased relative to that in SE mice (Fig. 4B).

We hypothesized that EE promoted angiogenesis, at least in part, through Ly6C^{low} macrophages since Ly6C^{low} macrophages can secrete angiogenic factors for tissue repair following MI (*24*). To test this hypothesis, we isolated Ly6C^{low} macrophages from infarcted hearts to facilitate the detection of angiogenesis-related gene expression. The results showed that *Vegf* expression in the EE-housed group was significantly higher than that in the SE-housed group (Fig. 4C), with immunostaining of tissues and sorted cells confirming a reduction in VEGF expression in Ly6C^{low} macrophages from SE-housed mice compared with EE-housed mice (Fig. 4, D and E). In addition, the expression of VEGF and CD31 in the infarct area at 14 days after MI was markedly higher in EE-housed mice than in SE-housed mice (Fig. 4F). However, CD31 expression was significantly higher in the border zone, and VEGF expression showed an increased trend in the EE group compared with that in the SE group at 14 days after MI (fig. S10A). These findings indicated that EE promoted angiogenesis, at least in part, via Ly6C^{low} macrophages.

EE increases the survival of Ly6C^{low} macrophages and their CCR2$^-$MHCII^{low} subsets by inhibiting apoptosis

Given the findings that EE housing increased the number of Ly6C^{low} macrophages in infarcted hearts, we sought to elucidate whether this higher number was the result of a decrease in apoptosis or an increase in proliferation. TUNEL staining showed that macrophage

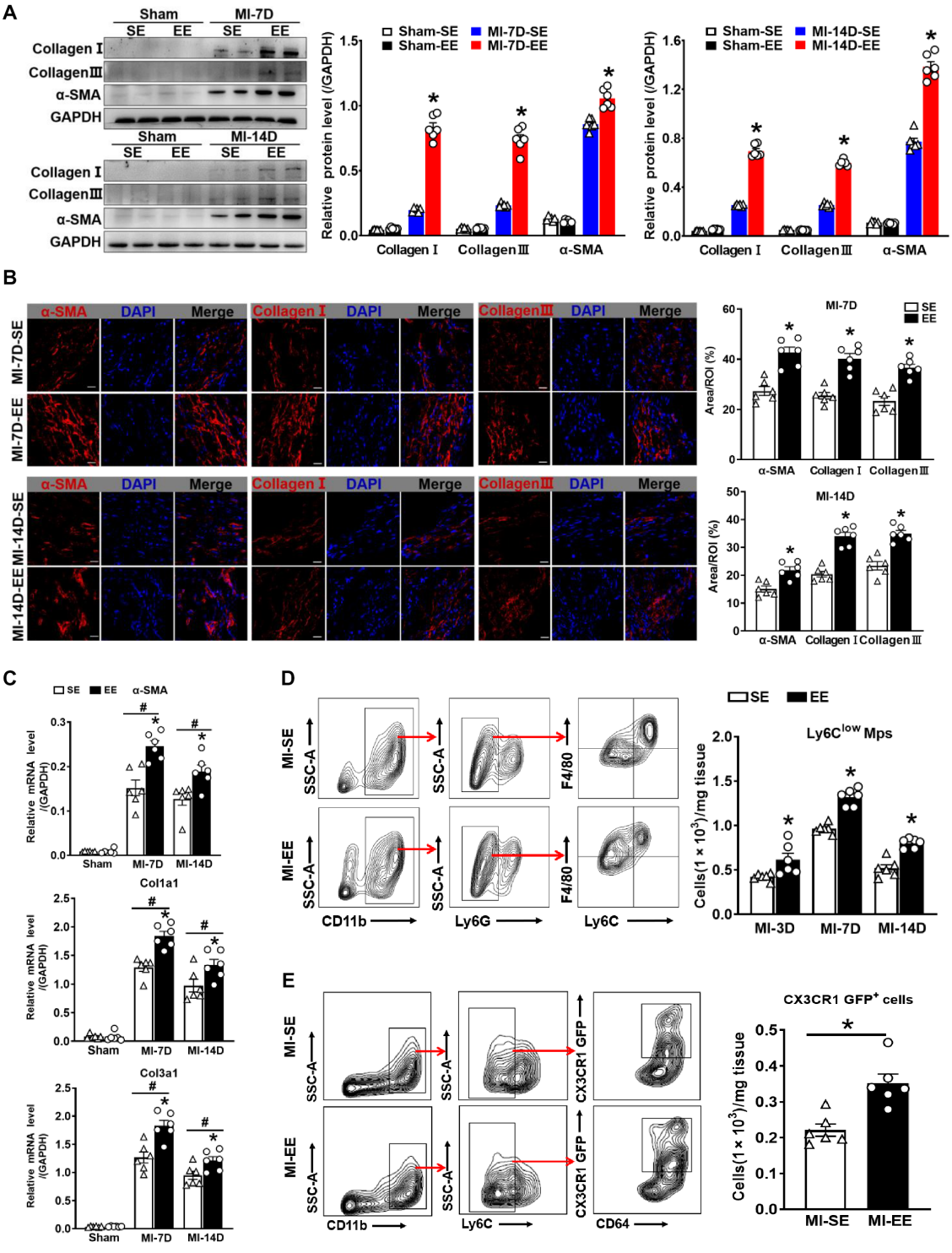

Fig. 3. EE promotes ECM synthesis and increases the number of Ly6C^{low} macrophages. (**A**) Western blot analyses of collagen I, collagen III, and α-SMA protein expression in the scar tissues of SE and EE mice at days 7 and 14 after MI or sham surgery ($n = 6$). *$P < 0.05$ versus SE-MI. GAPDH, glyceraldehyde-3-phosphate dehydrogenase (**B**) Immunostaining analyses of α-SMA, collagen I, and collagen III in the infarct area of SE and EE mice. Scale bars, 20 μm. *$P < 0.05$ versus SE. (**C**) mRNA expression of α-SMA, collagen 1a1 (Col1a1), and Col3a1 in the scar tissues of SE and EE mice at days 7 and 14 after MI or sham surgery ($n = 6$). #$P < 0.05$ versus sham. *$P < 0.05$ versus SE. (**D**) Gating strategy for Ly6C^{low} Mps and Ly6C^{high} Mos/Mps in hearts after MI. Flow cytometry–based quantification of Ly6C^{low} Mps at days 3, 7, and 14 after MI ($n = 5$ to 6). *$P < 0.05$ versus SE. (**E**) Gating strategy for CD45$^+$CD11b$^+$Ly6C$^-$CD64$^+$CX3CR1-GFP$^+$ macrophages of SE- and EE-housed CX3CR1-GFP mice at day 14 after MI. Quantification of CX3CR1-GFP$^+$ macrophages ($n = 6$). *$P < 0.05$ versus SE. Data are expressed as means ± SEM. Data in (**C**) were analyzed using two-way ANOVA followed by Bonferroni post hoc analysis. Data in (A), (B), (D), and (E) were analyzed using Student's *t* test.

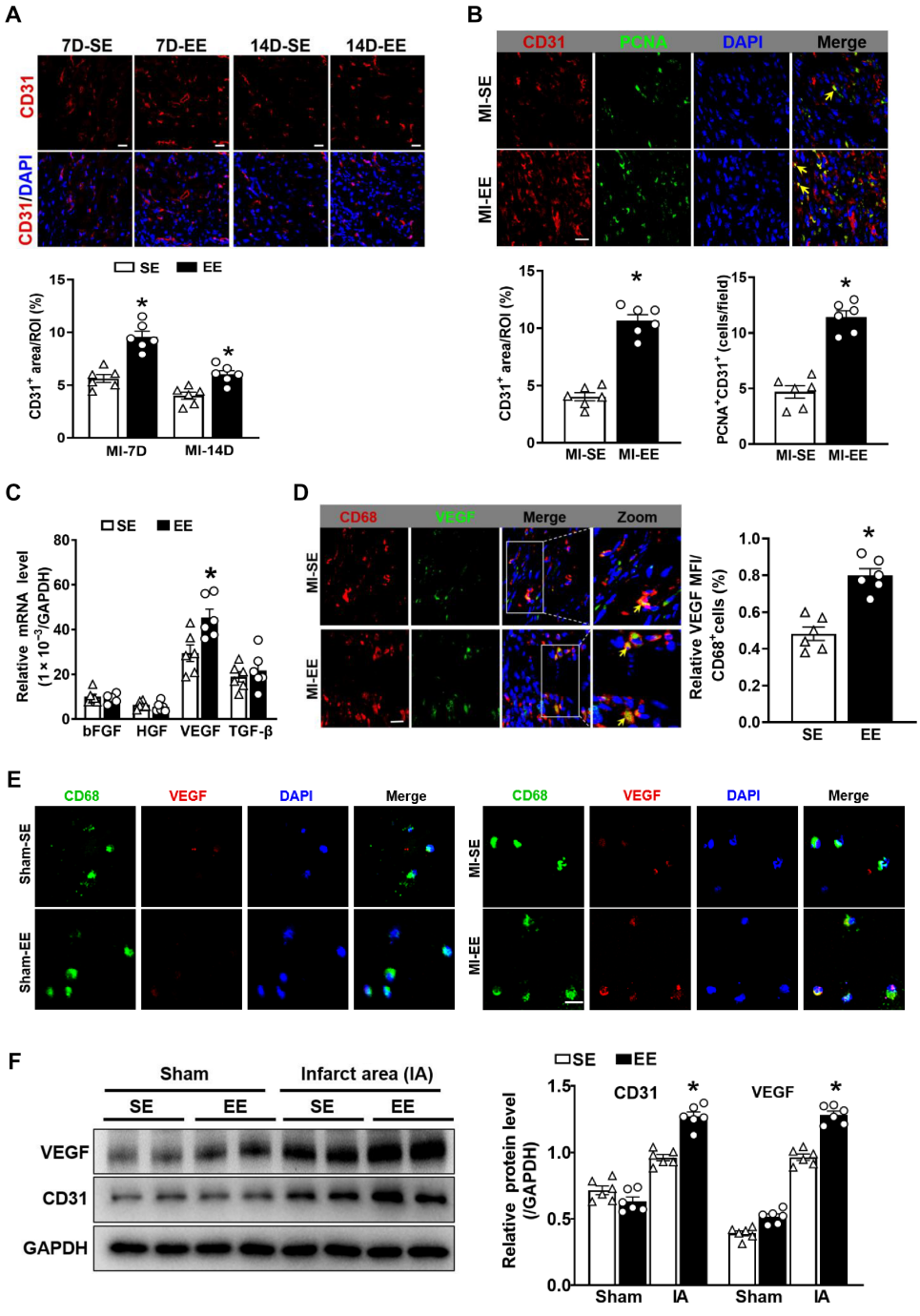

Fig. 4. EE promotes angiogenesis in infarct by VEGF secreted from Ly6C^{low} macrophages. (**A**) Immunostaining analyses of CD31 in infarct tissue collected at 7 and 14 days after MI. Scale bars, 20 μm. *$P < 0.05$ versus SE. (**B**) Immunostaining of CD31 (red) and PCNA (green) in the infarct zone. Scale bars, 20 μm. The yellow arrow indicates CD31$^+$/PCNA$^+$ cells. Quantitation of CD31$^+$ areas and CD31$^+$/PCNA$^+$ cells ($n = 6$). *$P < 0.05$ versus SE. (**C**) mRNA expression levels of fibroblast growth factor (FGF), hepatocyte growth factor (HGF), VEGF, and TGF-β in Mos/Mps sorted from hearts in SE-treated and EE-treated mice at day 7 after MI. *$P < 0.05$ versus SE. (**D**) Immunostaining for CD68 (red) and VEGF (green) in infarct tissue from SE and EE mice at day 7 after MI. Scale bars, 20 μm. The solid box outlines the region enlarged to the right. The yellow arrow indicates CD68$^+$/VEGF$^+$ cells. Quantitation of VEGF signaling in CD68$^+$ cells ($n = 6$). *$P < 0.05$ versus SE. (**E**) Representative immunostaining for CD68 (green) and VEGF (red) in Mos/Mps sorted from hearts of SE- and EE-treated mice at day 7 after MI or sham operation. Scale bars, 50 μm. (**F**) Western blot analyses of VEGF and CD31 expression in the infarct tissue of SE and EE mice at day 14 after MI or sham surgery. IA indicates infarct area. $N = 6$. *$P < 0.05$ versus SE. Data are expressed as means ± SEM. Data were analyzed using Student's *t* test.

survival was significantly higher in the hearts of EE mice than in SE-housed mice following MI (Fig. 5A). Concordant with improved survival, we also detected lower levels of active caspase-3 in Ly6C^{low} macrophages isolated from EE mice relative to SE mice (Fig. 5B). In addition, CD68 and Ki67 costaining to detect the proliferation of macrophages in situ or those isolated from infarcted tissues indicated no significant difference in macrophage proliferation between the EE and SE groups (fig. S11, A and B).

Recently, Epelman *et al.* (*25*) reestablished CD45, CD11b, CD64, CCR2, and major histocompatibility complex II (MHCII) as surface markers of mouse cardiac macrophages based on lineage tracing, flow cytometry, and transcriptomics analysis. Combining these new

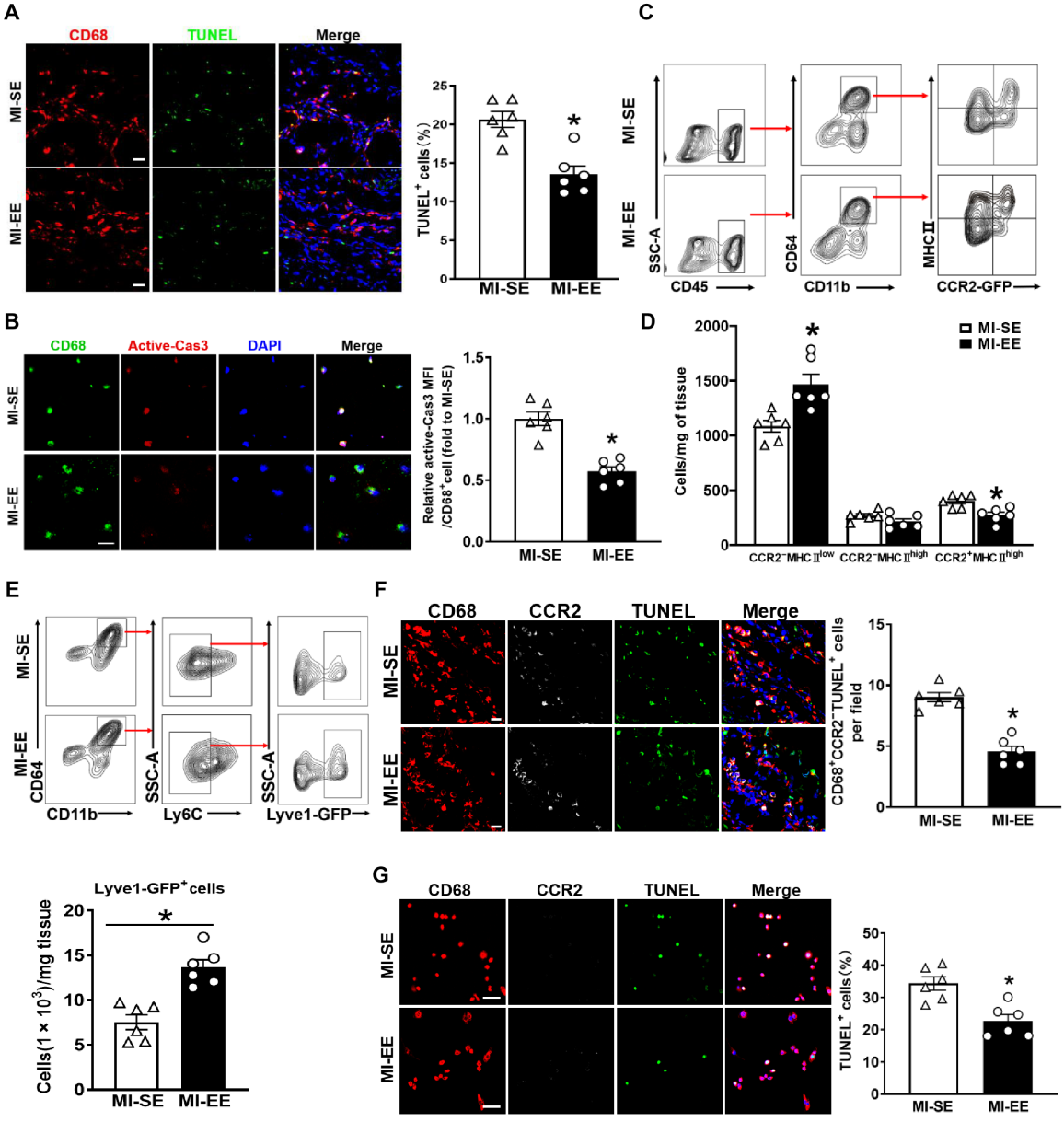

Fig. 5. EE promotes cardiac healing after MI by enhancing the survival of Ly6C^{low} macrophages and their CCR2^{-}MHCII^{low} subsets. (**A**) Immunostaining for CD68 (red) and TUNEL (green) in infarct zones of SE and EE mice at day 14 after MI. Scale bars, 20 μm. The percentage of TUNEL^{+} cells is expressed as TUNEL^{+}CD68^{+} cells/CD68^{+} cells. *P < 0.05 versus MI-SE. (**B**) Immunostaining for CD68 (green) and active caspase-3 (red) in Ly6C^{low} macrophages sorted from hearts of SE and EE mice at day 7 after MI. Scale bars, 50 μm. (**C**) Gating strategy for CD11b^{+}CD64^{+} macrophages and its subsets in hearts of SE and EE mice after MI. (**D**) Quantification of CCR2^{-}MHCII^{low}, CCR2^{-}MHCII^{high}, and CCR2^{+}MHCII^{high} macrophages as shown in (C) (n = 6). *P < 0.05 versus MI-SE. (**E**) Gating strategy for CD11b^{+}CD64^{+}Ly6C^{-}Lyve1-GFP^{+} macrophages in infarct tissues from Lyve1$^{EGFP\text{-}Cre}$ mice at day 14 after MI. Quantification of Lyve1-GFP^{+} macrophages (n = 6). *P < 0.05 versus MI-SE. (**F**) Immunostaining for CD68 (red), CCR2 (white), and TUNEL (green) in infarct zones of hearts from SE and EE mice at day 14 after MI. Scale bars, 20 μm. The percentage of CD68^{+}CCR2^{-}TUNEL^{+} cells is expressed as CD68^{+}CCR2^{-}TUNEL^{+}cells/CD68^{+} cells (n = 6). *P < 0.05 versus MI-SE. (**G**) Representative immunostaining for CD68 (red), CCR2 (white), and TUNEL (green) in CCR2^{-}MHCII^{low} macrophages sorted from infarcted hearts at day 7 after MI from SE- and EE-treated mice. The percentage of TUNEL^{+} cells is expressed as TUNEL^{+}CD68^{+} cells/CD68^{+} cells (n = 6). *P < 0.05 versus MI-SE. Data are expressed as means ± SEM. Data were analyzed using Student's t test. Scale bars, 50 μm.

molecules with previously published flow cytometry gating schemes, we classified macrophages into three subtypes: CCR2^{-}MHCII^{low}, CCR2^{-}MHCII^{high}, and CCR2^{+}MHCII^{high}. Following MI, the number of CCR2^{-}MHCII^{low} macrophages was significantly higher in EE-housed mice than in SE-housed mice (Fig. 5, C and D). On the basis of previous studies, cardiac resident macrophages, an important subset of CCR2^{-}MHCII^{low} macrophages after MI, specifically express higher levels of lymphatic vessel endothelial hyaluronan receptor 1 (Lyve1) (*26*, *27*). Therefore, to further determine the effect of EE on CCR2^{-}MHCII^{low} macrophages, we used Lyve1$^{EGFP\text{-}Cre}$ mice, which enabled us to observe cells expressing Lyve1. As expected, the number of Lyve1-GFP^{+} cells was significantly higher in EE mice than in SE mice (Fig. 5E). Moreover, we evaluated apoptosis by immunostaining for CD68, CCR2, and TUNEL staining, with the results demonstrating marked decreases in apoptosis in situ in the infarct tissue and in isolated CCR2^{-}MHCII^{low} macrophages within the EE group compared with the SE group (Fig. 5, F and G). These data verified that EE promoted the survival of Ly6C^{low} macrophages and their CCR2^{-}MHCII^{low} subsets predominantly by reducing apoptosis.

Cardiac resident macrophage ablation impairs the cardioprotective effect of EE

To determine the role of cardiac resident macrophages in EE-mediated cardioprotection, we used Cx3cr1^{CreER}×R26$^{Td/DTR}$ mice to selectively label and deplete resident macrophages (*26*). Three-week-old Cx3cr1^{CreER}×R26$^{Td/DTR}$ mice were fed tamoxifen (TAM)-chow for 10 days, which was then discontinued for 6 weeks. Daily diphtheria toxin (DT) injections were initiated 1 week before EE or SE induction to deplete and inhibit the numerical recovery of resident macrophages (Fig. 6, A and B). Notably, we observed that the lack of resident macrophages had little effect on other cell types (fig. S12).

We observed significantly enhanced cardiac function in the EE group relative to the SE group in control mice and consistent with our previous findings; however, the protective effect of EE on cardiac function was significantly reduced upon depletion of resident macrophages (Fig. 6, C and D). In addition, after the depletion of resident macrophages, the improved effect of EE on pulmonary edema and congestive heart failure after MI was significantly weakened (fig. S13A). TC staining showed that EE significantly reduced the infarct size and increased wall thickness compared with SE at 14 days after MI in control mice, whereas EE failed to improve cardiac remodeling after ablation of resident macrophages (Fig. 6E). Further studies confirmed that enhanced ECM protein deposition and angiogenesis under EE conditions were significantly reduced after depletion of resident macrophages (Fig. 6, F and G, and fig. S13B). Collectively, these data indicated that resident macrophages are indispensable to the cardioprotective effect of EE.

EE-mediated cardiac repair is associated with increased BDNF expression in the hypothalamus

To further explore the underlying mechanisms by which EE promoted the survival of CCR2^{-}MHCII^{low} macrophages, we screened several key molecules associated with immune metabolism in the hypothalamus, a brain area closely linked with the effects of the EE (*28*). The results showed that BDNF expression in the EE group was significantly higher than that in the SE group after MI (Fig. 7A). In addition, BDNF expression was higher in the hypothalamus than that in the bone marrow, spleen, and heart (Fig. 7B), and enzyme-linked immunosorbent assay (ELISA) results indicated that plasma BDNF content in EE mice was significantly higher than that in SE mice after MI (Fig. 7C). On the basis of these findings, we speculated that EE promotes BDNF expression in both the hypothalamus and plasma after MI and thus participates in the regulation of myocardial macrophages.

Immunoblotting also confirmed that the BDNF expression in the infarct area of EE mice was slightly higher than that in SE mice (Fig. 7D). Studies have confirmed that BDNF performs its functions mainly by binding to its receptor, tropomyosin receptor kinase B (TrkB) (*29*). In the present study, the expression of TrkB in infarcted tissues did not differ significantly between the two groups (Fig. 7D); however, by analyzing the subsets of cells in the heart, we found that TrkB expression in CCR2^{-}MHCII^{low} macrophages (M2) was significantly higher than that in endothelial cells, cardiomyocytes, and fibroblasts following MI (Fig. 7, E and F). The BDNF-TrkB axis reportedly activates the extracellular signal–regulated kinase 1/2 (ERK1/2) and AKT pathways, thereby inhibiting apoptosis and promoting cell survival (*30*). Immunostaining demonstrated that CCR2^{-}MHCII^{low} macrophages isolated from the hearts of EE mice harbored higher levels of phosphorylated ERK (p-ERK) and p-AKT compared with hearts from SE mice (Fig. 7G and fig. S13C). In addition, we observed increased expression of the antiapoptosis molecule B cell lymphoma 2 (BCL-2) and decreased expression of the proapoptosis molecule BCL-2–associated X protein (Bax) in CCR2^{-}MHCII^{low} macrophages sorted from EE mice compared with that in SE mice (Fig. 7H and fig. S13D). We also observed that ANA-12, a selective inhibitor of TrkB, significantly impaired EE-induced improvements in cardiac function and ventricular remodeling (fig. S13, E to G). Collectively, these data suggested that higher plasma BDNF levels, associated with BDNF up-regulation in the hypothalamus, promoted the survival of cardiac macrophages by binding to its receptor TrkB (Fig. 7I).

Hypothalamic BDNF knockdown inhibits EE-induced cardiac repair

To further confirm that hypothalamus-derived BDNF is a key mediator of EE-mediated protective effects on cardiac repair, we injected recombinant adeno-associated virus (rAAV)-U6-short hairpin (sh) RNA(BDNF)-CMV-EGFP or adeno-associated virus (AAVs) encoding the control short hairpin RNA (shRNA) into the hypothalamic region of mice to interfere with BDNF expression (Fig. 8A). Mice were euthanized 4 weeks after the virus injection, and the hypothalamus was isolated. Immunoblotting showed that BDNF expression in the hypothalamus was significantly lower in rAAV-U6-shRNA(BDNF)-CMV-EGFP–injected mice (hereafter HBKD mice) than rAAV-U6-shRNA(scramble)-CMV-EGFP–injected mice (hereafter control mice) (Fig. 8B).

Moreover, ELISA results showed that EE treatment significantly increased plasma BDNF levels in control mice; however, this effect was significantly inhibited in HBKD mice (Fig. 8C). Notably, although cardiac function (EFs) was significantly enhanced in the EE group relative to the SE group in control mice, the EE-mediated enhancement of cardiac function was significantly inhibited in HBKD mice (Fig. 8D). In addition, TC staining showed that EE significantly reduced the infarct size and increased wall thickness compared with that observed in the SE group at 14 days after MI in control mice, whereas EE failed to improve cardiac remodeling in HBKD mice (Fig. 8E). Furthermore, immunostaining, Western blotting, and qPCR revealed that BDNF knockdown in the hypothalamus inhibited EE-mediated enhancements in ECM protein deposition and

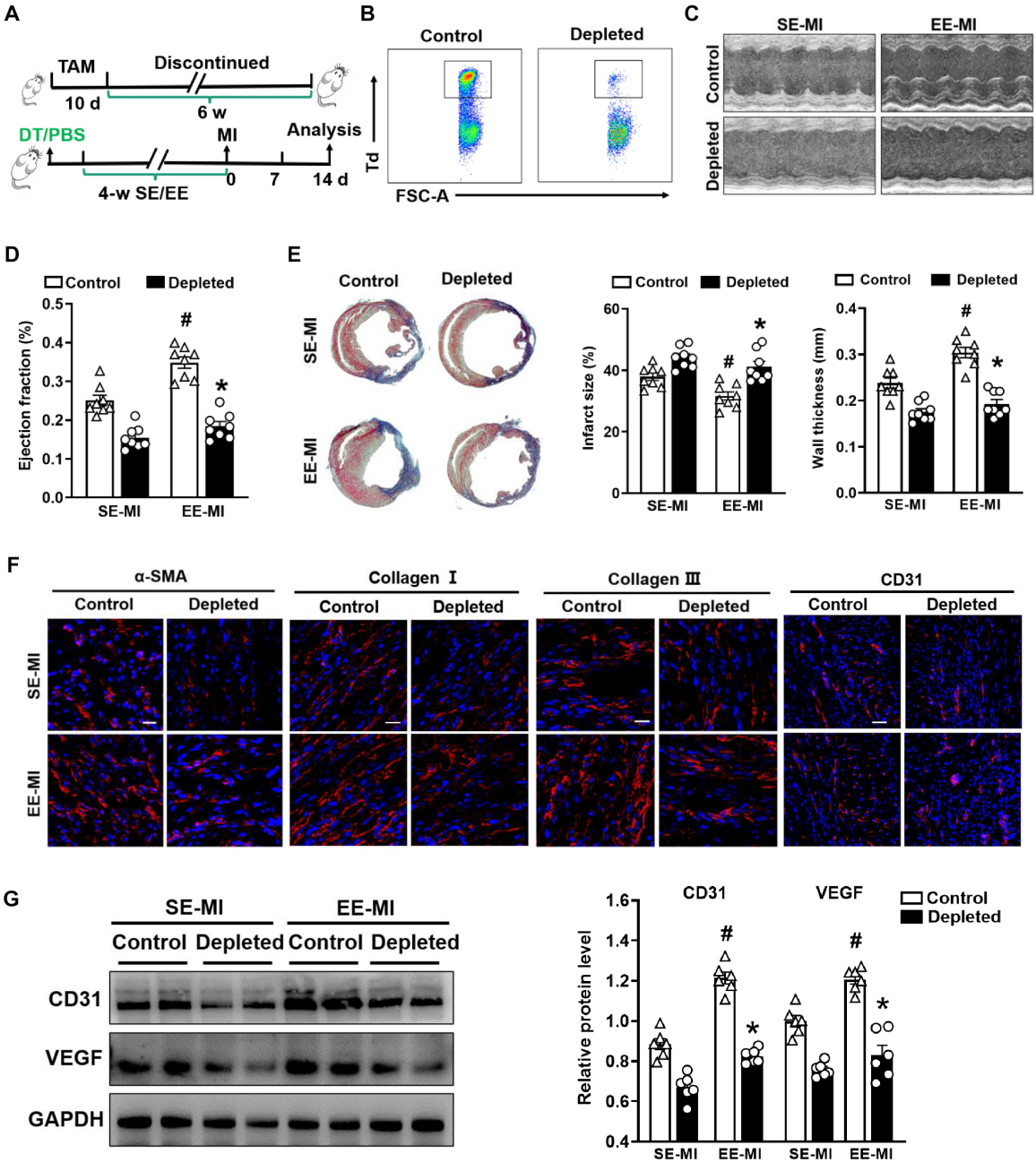

Fig. 6. Depletion of cardiac resident macrophages impairs the EE-mediated cardioprotective effect. (**A**) Timeline diagram of the experimental procedures. (**B**) Representative flow cytometric plots of Td^+ resident macrophages following the administration of DT to $Cx3cr1^{CreER}\times R26^{Td/DTR}$ and $Cx3cr1^{CreER}\times R26^{Td/+}$ mice. (**C** and **D**) Echocardiographic analysis of EF value at day 14 after MI after SE and EE housing ($n = 8$). #$P < 0.05$ versus SE-MI. *$P < 0.05$ versus control. (**E**) Representative Masson's staining of cardiac tissue obtained from depleted and control mice 14 days after MI. Quantitative analysis of infarct size and wall thickness ($n = 8$). #$P < 0.05$ versus SE-MI. *$P < 0.05$ versus control. (**F**) Immunostaining analyses of α-SMA, collagen I, collagen III, and CD31 on infarct sections collected at 14 days after MI. Scale bars, 20 μm (for α-SMA, collagen I, and collagen III) and 50 μm (for CD31). (**G**) Western blot analyses of VEGF and CD31 expression in the infarct tissues at day 14 after MI ($n = 6$). #$P < 0.05$ versus SE-MI. *$P < 0.05$ versus control. Data are expressed as means ± SEM. Data were analyzed using Student's *t* test.

angiogenesis (Fig. 8, F to I, and fig. S14, A to C). Flow cytometry also confirmed no significant difference in the number of $CCR2^{-}MHCII^{low}$ macrophages in HBKD mice between SE and EE groups, whereas control mice showed a markedly higher number of $CCR2^{-}MHCII^{low}$ macrophages after EE treatment (Fig. 8J).

Hypothalamic BDNF infusion mimics EE-induced cardioprotective effects

We then evaluated the effect of hypothalamic BDNF infusion on MI repair (fig. S15A). TC staining showed that BDNF-treated mice displayed reduced infarct size and increased wall thickness at day 14

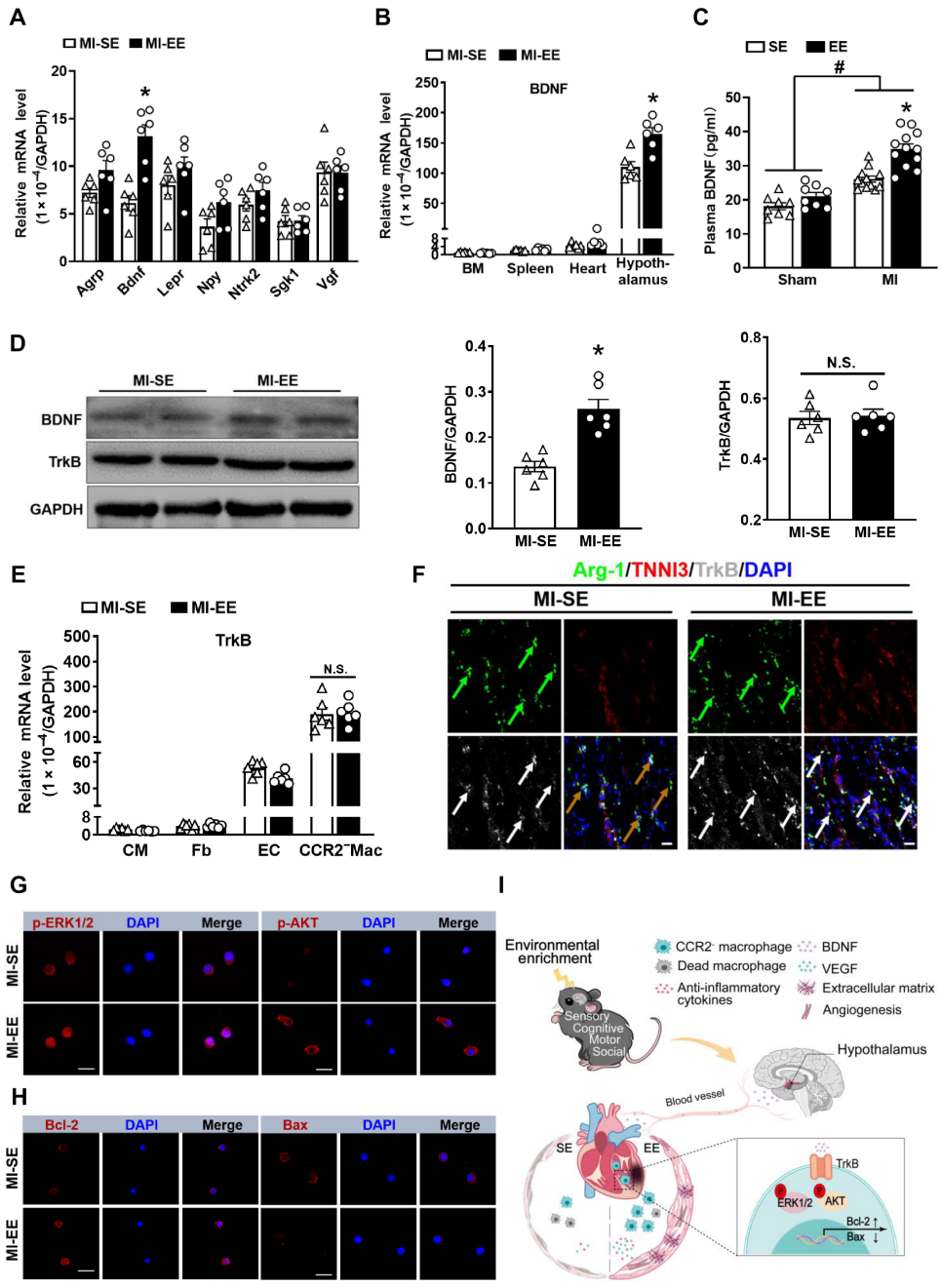

Fig. 7. EE promotes CCR2^{-}MHCII^{low} macrophage survival via the BDNF-TrkB axis. (**A**) mRNA expression of agouti-related peptide (*Agrp*), *Bdnf*, leptin receptor (*Lepr*), neuropeptide Y (*Npy*), neurotrophic receptor tyrosine kinase 2 (*Ntrk2*), serum/glucocorticoid-regulated kinase1 (*Sgk1*), and nerve growth factor inducible (*Vgf*) in hypothalamus obtained from SE and EE mice at day 7 after MI ($n = 6$). *$P < 0.05$ versus SE. (**B**) mRNA expression of *BDNF* in bone marrow (BM), spleen, heart, and hypothalamus collected from SE and EE mice at day 7 after MI ($n = 6$). *$P < 0.05$ versus SE. (**C**) The BDNF content in plasma of SE- and EE-housed mice at day 14 after MI or sham operation. *$P < 0.05$ versus SE and #$P < 0.05$ versus sham. (**D**) Western blot analyses of BDNF and TrkB expression in the infarct tissues at day 14 after MI ($n = 6$). *$P < 0.05$ versus MI-SE. (**E**) *TrkB* mRNA expression in cardiomyocytes (CMs), fibroblasts (Fb), endothelial cells (ECs), and CCR2^{-}MHCII^{low} macrophages sorted from the hearts at day 7 after MI ($n = 6$). *$P < 0.05$ versus MI-SE. (**F**) Immunostaining analyses of Arg-1, cardiac troponin I (TNNI3), and TrkB on infarct sections collected at 14 days after MI. Scale bars, 20 μm. (**G**) Immunostaining of p-ERK1/2 and p-AKT in CCR2^{-}MHCII^{low} macrophages sorted from infarcted hearts. Scale bars, 50 μm. (**H**) Immunostaining of Bcl-2 and Bax in CCR2^{-}MHCII^{low} macrophages sorted from the infarcted hearts. Scale bars, 50 μm. (**I**) Mechanism of EE-induced cardioprotective effect in mice after MI.Data are expressed as means ± SEM. Data in (C) were analyzed using two-way ANOVA followed by Bonferroni post hoc analysis. Data in (A), (B), (D), and (E) were analyzed using Student's *t* test.

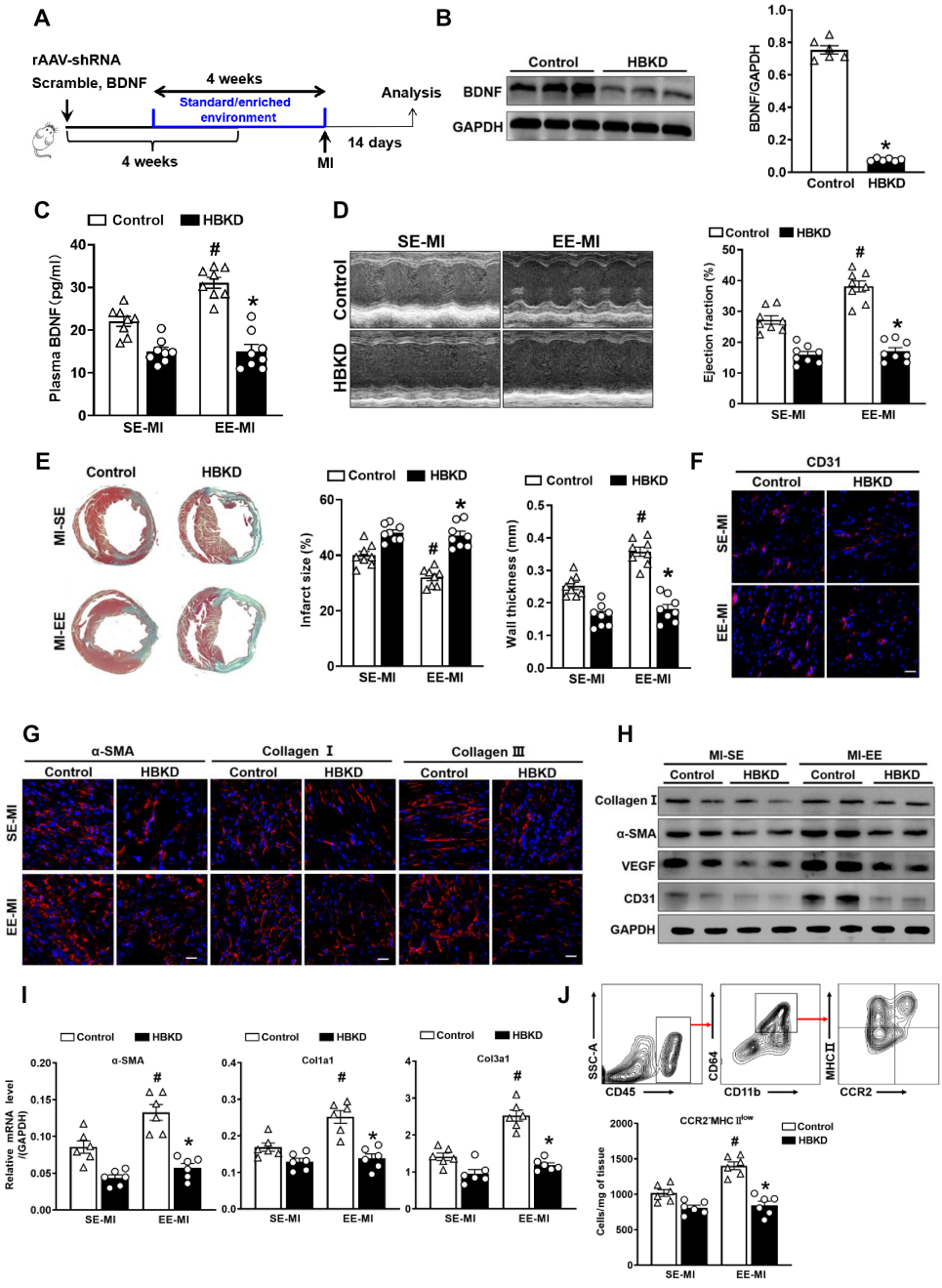

Fig. 8. Hypothalamic BDNF knockdown inhibits EE-induced cardiac repair. (**A**) Timeline diagram of the experimental procedures. (**B**) Western blot analysis of BDNF expression in the hypothalamus between HBKD and control mice 4 weeks after the virus injection ($n = 6$). *$P < 0.05$ versus control. (**C**) The BDNF content in plasma of HBKD and control mice at day 14 after MI after SE and EE housing. #$P < 0.05$ versus SE-MI. *$P < 0.05$ versus control. (**D**) Echocardiographic analysis of EF value of HBKD and control mice at day 14 after MI after SE and EE housing ($n = 8$). #$P < 0.05$ versus SE-MI and *$P < 0.05$ versus control. (**E**) Masson's staining of cardiac tissue obtained from HBKD and control mice at day 14 after MI after SE and EE housing. Quantitative analysis of infarct size and wall thickness ($n = 8$). #$P < 0.05$ versus SE-MI. *$P < 0.05$ versus control. (**F** and **G**) Immunostaining analyses of CD31, α-SMA, collagen I, and collagen III on infarct sections collected at 14 days after MI. Scale bars, 50 μm (for CD31) and 20 μm (for α-SMA, collagen I, and collagen III). (**H**) Representative Western blot analyses of collagen I, α-SMA, VEGF, and CD31 expression in the infarct tissues at day 14 after MI ($n = 6$). (**I**) mRNA expression of *α-SMA*, *Col1a1*, and *Col3a1* in scar tissues at day 14 after MI. #$P < 0.05$ versus SE-MI. *$P < 0.05$ versus control. (**J**) Gating strategy and quantification of $CCR2^{-}MHCII^{low}$ macrophages in the hearts of HBKD and control mice after MI ($n = 6$). #$P < 0.05$ versus SE-MI. *$P < 0.05$ versus control.

after MI compared with control mice (fig. S15B). In addition, BDNF-treated mice exhibited significantly higher cardiac function than vehicle-treated mice after MI (fig. S15C). The ECM protein expression and angiogenesis were significantly higher in BDNF-treated mice than those in controls at day 14 after MI (figs. S15, D to G, and S16, A to C). Moreover, the infarct site in BDNF-treated mice contained more Arg-1^{+} macrophages than that in control mice (figs. S15H and S16D), and BDNF treatment reduced the apoptosis

of $CD68^+CCR2^-MHCII^{low}$ macrophages isolated from hearts at day 14 days after MI (fig. S16E). These findings demonstrated that the cardioprotective effect exerted by EE was at least partly associated with hypothalamic BDNF.

DISCUSSION

Psychosocial stress is critically involved in the pathogenesis of MI. Unlike distress, which has been extensively studied (*2*, *3*, *31*), the present study demonstrated that environmental eustress via an EE had protective effects on post-MI repair. Specifically, we found that EE improved cardiac function, reduced mortality, and limited adverse ventricular remodeling in experimental MI mice. Furthermore, the data confirmed that EE participated in cardiac repair after MI primarily by promoting the survival of $Ly6C^{low}$ macrophages and their $CCR2^-MHCII^{low}$ subsets mediated by BDNF.

EE has attracted long-standing interest as a model for studying eustress in recent years and is believed to allow the body to return to normal homeostasis under various stimuli (*9*, *32*). Studies revealed that EE can not only improve learning and memory and protect the brain from cognitive deficits caused by injury but also promote angiogenesis. For example, EE improves post-stroke angiogenesis by increasing the number of microvessels in the peri-infarct area (*33*). Moreover, mesenchymal stem cells combined with EE can attenuate brain injury by increasing endogenous angiogenesis and upregulating angiogenic factors (*34*). Regulation of the immune response is a crucial mechanism of EE associated with inhibiting the growth of melanoma, colon cancer, breast cancer, pancreatic cancer, and glioma in mice or rats (*6*). Collectively, the two critical mechanisms through which EE participates in these diseases are immune inflammation and angiogenesis, coincidentally, pivotal players in cardiac repair. Although EE reportedly mitigates the extent of atherosclerosis in apolipoprotein E-knockout mice and reduces the mean arterial pressure in rats with renovascular hypertension (*14*, *35*), this present study is the first regarding its role in MI. These findings provide sound theoretical support for the role of EE in cardiac repair after MI.

Similar to a previous study (*5*), we exposed mice to EE for 4 weeks before MI. As expected, EE-housed mice exhibited markedly reduced mortality, improved cardiac function, and optimized ventricular remodeling following MI. The quality of repair after MI is determined by ECM deposition and the inflammatory response (*36*). We observed significantly higher expression of ECM components, including collagen I, collagen III, and α-SMA, in EE mice. In addition, our data strongly support an intrinsic role for EE in promoting an immunosuppressive environment within the infarct site, as evidenced by the decreased expression of proinflammatory factors and increased expression of anti-inflammatory factors. We also examined dynamic variations in the inflammatory cells at the infarct site. In line with these results, the prevalence of proinflammatory M1-like macrophages declined, whereas the prevalence of anti-inflammatory M2-like macrophages increased significantly.

Furthermore, considering that classification of macrophages into M1 or M2 phenotypes is based on in vitro experiments (*37*), it cannot reflect the actual number and function of macrophages in vivo. However, Ly6C is a marker used widely in recent years to identify subgroups of macrophages with distinct roles in various diseases (*38*). Our flow cytometry analysis corroborated that EE could significantly increase the number of $Ly6C^{low}$ macrophages. Apart from promoting ECM synthesis, $Ly6C^{low}$ macrophages can also increase angiogenesis (*24*). Studies show that one of the mechanisms through which EE improves disease status involves the enhancement of angiogenesis (*34*, *39*). In the present study, we found significantly higher $Ly6C^{low}$ macrophage-mediated expression of CD31 and VEGF in the infarcted areas of EE-housed mice. Collectively, EE enhanced cardiac repair, at least partially, via reparative $Ly6C^{low}$ macrophages.

An increasing number of reports have recently asserted that infarcted hearts contain a broad spectrum of macrophage subsets with distinct properties and functional characteristics (*22*). Therefore, we evaluated whether EE critically regulated the function of each macrophage cluster. Epelman *et al.* (*25*) performed detailed lineage tracing, flow cytometry, and transcriptomics analyses to reestablish surface markers of mouse cardiac macrophages, with macrophages subsequently divided into three groups based on CCR2 and MHCII:$CCR2^-MHCII^{low}$, $CCR2^-MHCII^{high}$, and $CCR2^+MHCII^{high}$ (*26*). On the basis of this new classification, we observed that EE significantly increased the size of the $CCR2^-MHCII^{low}$ cluster. Collectively, these findings indicated that EE increased the amount of $Ly6C^{low}$ macrophages and their $CCR2^-MHCII^{low}$ subsets. Moreover, we used multiple transgenic mouse lines to further confirm these alterations. First, we used CX3CR1-GFP mice to indirectly determine whether EE increased the number of $Ly6C^{low}$ macrophages, contingent on the fact that $Ly6C^{low}$ macrophages express high levels of CX3CR1 (*24*). Furthermore, we used CCR2-GFP mice to study the effect of EE on $CCR2^-MHCII^{low}$ macrophages, with the results consistent with previous findings. The sources of $CCR2^-MHCII^{low}$ macrophages in infarcted tissues are complex, and the resident macrophages are an important part of them. Using single-cell sequencing technology to analyze different subsets of macrophages in the mouse heart and found that resident macrophages specifically express Lyve1 (*26*, *27*). Therefore, to further confirm the effect of EE on $CCR2^-MHCII^{low}$ macrophages, we exposed $Lyve1^{EGFP\text{-}Cre}$ mice to EE for 4 weeks and found that EE increased the number of Lyve1-$EGFP^+$ cells. Last, to determine the essential role of resident macrophages in EE-mediated cardiac protection, $Cx3cr1^{CreER}$ mice were crossed with $R26^{Td/DTR}$ mice to produce $Cx3cr1^{CreER}\times R26^{Td/DTR}$ mice, which allowed for Cre-mediated expression of DT receptor and rendered resident cardiac macrophages highly sensitive to DT (*40*). When exposed to DT, resident macrophages can be specifically ablated. We found that EE had a significant cardioprotective effect in control mice, whereas EE failed to improve cardiac remodeling in resident macrophage–depleted mice although showed a trend toward improvement. Possible explanations include the fact that EE promotes increased levels of circulating BDNF, which acts not only on cardiac macrophages but also on endothelial cells and cardiomyocytes to promote cardiac protection. In addition, EE has an interaction between the central nervous system, endocrine system, and immune system and might also partially regulate the heart through neuroendocrine factors (*28*, *41*). Collectively, using $Cx3cr1^{CreER}\times R26^{Td/DTR}$ mice and $Lyve1^{EGFP\text{-}Cre}$ mice, we confirmed the role of cardiac resident macrophages in EE-mediated cardiac protection, which can also indirectly reflect the role of $CCR2^-MHCII^{low}$ macrophages in EE-induced cardiac repair after MI.

Extensive evidence indicates that the cross-talk between the nervous and immune systems occurs via multiple pathways (*42*). EE comprises more elaborate housing along with sensory, cognitive, motor, and social stimulation, and this complexity is further manifested in the interactions among the central nervous, endocrine,

and immune systems (*28*, *41*). Moreover, EE significantly increases the expression of BDNF in the hypothalamus, the primary mediator of EE involved in many diseases (*5*, *28*). In the present study, we observed elevated BDNF expression in the hypothalamus of EE mice, and ELISA revealed that plasma BDNF levels in EE mice were significantly higher than those in SE mice after MI. Peripheral responses elicited by central nervous system activation might play an important role in the progression or prevention of cardiac remodeling after MI (*30*). ###The results suggest that EE promotes hypothalamic BDNF expression, further affecting plasma BDNF levels and acting on cardiac macrophages. BDNF predominantly functions via the receptor TrkB (*43*). In support of this assertion, we found that $CCR2^{-}MHCII^{low}$ macrophages expressed higher levels of TrkB than endothelial cells, cardiomyocytes, and fibroblasts following MI. We also observed that ANA-12, a selective inhibitor of TrkB (*44*), significantly impaired EE-mediated cardiac repair after MI. Moreover, BDNF/TrkB signaling reportedly mediates activation of the mitogen-activated protein kinase and AKT pathways (*43*, *45*). We observed higher p-ERK1/2 and p-AKT levels in $CCR2^{-}MHCII^{low}$ macrophages. ###To further confirm that hypothalamus-secreted BDNF is closely associated with EE-induced cardioprotective effects, we knocked down BDNF expression in the hypothalamus by in situ injection of AAVs. As expected, we observed that EE exerted effective cardiac repair functions in control mice but lost this effect following BDNF knockdown. Furthermore, BDNF infusion into the hypothalamus via an osmotic pump optimized wound healing, demonstrating that increased BDNF expression in the hypothalamus can simulate the EE-mediated effect. Collectively, these results indicated that the mechanisms through which EE promotes cardiac repair are closely associated with increased BDNF expression in the hypothalamus.

There are some limitations to this study. We relied on animal models rather than clinical patient data, which will need to be integrated in the future to validate these results. Furthermore, there are currently no consistent standards for EE models, and this lack of consistency may lead to variation in results across studies. Nevertheless, we have demonstrated that optimal cardiac repair in EE-housed mice is correlated with BDNF-mediated cardiac macrophage survival. Thus, this study has great significance in providing a new strategy for delaying adverse remodeling following MI.

METHODS

Mice

$CX3CR1^{GFP/GFP}$, $CCR2^{GFP/GFP}$, $Lyve1^{EGFP\text{-}Cre}$, $Cx3cr1^{CreER}$, and $R26^{Td/DTR}$ mice were purchased from the Jackson Laboratory. Male wild-type (WT) mice (C57BL/6, 3 to 4 weeks old) from Model Organisms Center Inc. (Shanghai, China) were used in this study. $CX3CR1^{GFP/+}$ mice were generated by crossing $CX3CR1^{GFP/GFP}$ mice with WT mice. Similarly, $CCR2^{GFP/GFP}$ mice were crossed with WT mice to generate $CCR2^{GFP/+}$ mice. To obtain $Cx3cr1^{CreER}$×$R26^{Td/DTR}$ mice, $Cx3cr1^{CreER}$ mice were crossed with $R26^{Td/DTR}$ mice. The $Cx3cr1^{CreER}$×$R26^{Td/DTR}$ mice exhibited selective depletion of Td^{+} cells following administration of DT. Because previous studies demonstrated a protective effect of estrogen against ischemic cardiac injury and therefore suggested the male sex as an important risk factor for cardiovascular disease (*46*), only male mice were used in this study. This study and all the animal experimental procedures followed the Institutional Animal Care and Use Committee guidelines of Fudan University.

EE model

Male mice (3 to 4 weeks old) were randomly assigned to either SE or EE housing for 4 weeks before MI surgery. As previously described (*28*), SE housing consisted of standard laboratory cages, each housing five mice, whereas EE housing included richness, novelty, and sociality elements. Specifically, the EE cages were larger and accommodated 12 mice at a time to ensure a certain degree of sociality. The EE cages were also equipped with various toys, including running wheels, tunnels, wooden toys, small huts, and nesting materials, to maintain environmental richness. In addition, the layout of the elements was changed once a week, and the relative position of the toys was changed every 3 days to maintain the novelty of the environment. Following MI surgery, the mice continued to be housed under their respective environments until the end of the experiment.

MI model

Mice were subjected to permanent LAD artery ligation or sham surgery, as previously described (*24*). Briefly, mice were anesthetized using 1.5% isoflurane and fixed to the operating table. A 1.2-cm longitudinal incision was made over the lower-left sternum of each mouse, and the chest muscles and subcutaneous tissues were separated. The fourth intercostal space was exposed, and the chest cavity was gently squeezed to expose the heart. The LAD artery was then ligated approximately 3 mm from the left auricle with a 6-0 silk thread. Successful ligation was confirmed by observing a pallor of the anterior wall of the ventricle and by the presence of an ST-segment elevation on an electrocardiogram. The heart was reset immediately after ligation. The air was removed from the chest cavity. Each muscle layer was resealed, and the skin was sutured with a 4-0 silk thread. After surgery, mice were placed on a heating pad until they recovered. For sham surgery, the LAD artery was not ligated. Mice that died within 24 hours of the surgery were excluded from the study.

Ablation of cardiac resident macrophages

We crossed $Cx3cr1^{CreER}$ mice with $R26^{Td/DTR}$ mice to obtain mice expressing resident cardiac macrophage–specific DT receptor (DTR), making these macrophages susceptible to DT-induced cell death (*26*, *47*). Briefly, 3-week-old $Cx3cr1^{CreER}$×$R26^{Td/DTR}$ mice were fed TAM-chow for 10 days and then discontinued for 6 weeks. Daily DT injections were administered 1 week before EE or SE induction to deplete and inhibit the numerical recovery of resident macrophages. Briefly, 500 ng of DT was administered intraperitoneally daily for the first 7 days, followed by 250 ng intraperitoneally daily until 14 days after MI. After administering the injection for 1 week, tissue samples were collected to test for knockout efficiency. The $Cx3cr1^{CreER}$×$R26^{Td/DTR}$ mice and $Cx3cr1^{CreER}$×$R26^{Td/+}$ mice were kept in EE or SE housing for 4 weeks before MI surgery.

Echocardiography

Cardiac function was evaluated at different time points using a Vevo 2100 system (VisualSonics, Toronto, Canada), as previously described (*22*). Specifically, mice were anesthetized using isoflurane and fixed in the supine position to a 37°C constant-temperature operation table. To reduce data bias, a low dose of isoflurane was used so that the mice could remain slightly conscious during the image acquisition process. The EDV and ESV were determined using the biplane area-length method. The LVEF was calculated using the following formula: LVEF (%) = [(EDV − ESV)/EDV] × 100%. Two-dimensional M-mode images were obtained in the long- and

short-axis views to measure LVEDD and LVESD. The FS was calculated using the following formula: FS (%) = [(LVEDD − LVESD)/LVEDD] × 100%. To eliminate bias, the operator was blinded to group assignment during image analysis.

Histological analyses

Heart tissues were fixed overnight in 4% paraformaldehyde and then embedded in paraffin. The paraffin-embedded tissues were sectioned into 5-μm-thick slices. H&E, Masson's trichrome, and Picrosirius red staining assays were performed on the paraffin-embedded sections to identify morphological changes and the degree of fibrosis. Infarction size was calculated as total infarction circumference/total LV circumference × 100%. Collagen density was evaluated as the ratio of positive staining area to the total scar area. Ten to 15 images were collected from different fields of each tissue section. Images were analyzed using the ImageJ software (National Institutes of Health, Bethesda, MD, USA). To eliminate bias, the researcher was blinded to group assignment during image analysis.

Immunofluorescence analyses

Cardiac tissue sections were selected for further immunofluorescence analysis as previously described (*22*). The paraffin sections were deparaffinized, hydrated, and then subjected to sodium citrate antigen retrieval. The subsequent steps were similar to those used for processing the frozen sections. Specifically, after rinsing with PBST (phosphate-buffered saline with Tween 20), nonspecific binding was blocked with 5% bovine serum albumin. The sections were then incubated overnight at 4°C with specific primary antibodies. The following primary antibodies were used: α-SMA (A5228; Sigma-Aldrich, St. Louis, MO, USA), collagen 1a1 (NBP1-30054; Novus Biologicals, Littleton, CO, USA), collagen 3a1 (ab7778, Abcam), F4/80 (ab6640, Abcam), CD68 (ab53444, Abcam), VEGF (sc-7269, Santa Cruz Biotechnology, CA, USA), Ki67 (ab15580; Abcam), CCR2 (ab203128, Abcam), cardiac troponin I (TNNI3) (SAB2502170, Sigma-Aldrich), CD31 (ab222783, Abcam), and BDNF (ab108319, Abcam). Sections were incubated with fluorescent secondary antibodies for 2 hours at room temperature. After 4′,6-diamidino-2-phenylindole staining, the sections were treated with antiquenching reagent and observed under a laser scanning confocal microscope (Carl Zeiss, Oberkochen, Germany). For each section, 10 to 15 fields were randomly selected, and the Zeiss software system was used for subsequent image processing.

Enzyme-linked immunosorbent assay

The mice were euthanized, and the blood samples were collected into EDTA-containing tubes. Plasma was separated by centrifugation at 1600*g*, for 15 min at 4°C. The supernatant was frozen at −80°C until analyses. Plasma BDNF levels were then determined using the Mouse BDNF ELISA Kit (Boster Biological Technology Ltd., Wuhan, China), according to the manufacturer's instructions. After adding the stop solution, the optical densities were measured at 450 nm with a microplate reader.

Protein preparation and Western blot analysis

Western blot analysis was performed as previously described (*15*). Equal amounts of protein were separated by SDS–polyacrylamide gel electrophoresis gels and then transferred to a polyvinylidene difluoride membrane. The membrane was incubated with 5% skim milk to block nonspecific binding. Next, the membrane was washed with tris-buffered saline and incubated overnight at 4°C with the following specific primary antibodies: α-SMA (A5228, Sigma-Aldrich), collagen I (NBP1-30054, Novus Biologicals), collagen III (ab7778, Abcam), BDNF (ab108319, Abcam), VEGF (sc-7269, Santa Cruz Biotechnology), CD31 (AF3628, R&D Systems, Minneapolis, MN, USA), glyceraldehyde-3-phosphate dehydrogenase (GAPDH; 5174, Cell Signaling Technology). Species-specific horseradish peroxidase–conjugated secondary antibodies were used to bind the corresponding primary antibodies, and the signals were detected using an enhanced chemiluminescence reagent. The bands were analyzed using the ImageJ software.

RNA extraction and real-time PCR

Total RNA was isolated from heart tissues, hypothalamus tissues, cardiac fibroblasts, and cardiomyocytes using TRIzol reagent (15596018, Invitrogen), as previously described (*48*). RNA was isolated from endothelial cells and sorted macrophages using RNeasy Plus Micro Kit (74034, QIAGEN) according to the manufacturer's instructions. Briefly, total RNA (1 μg) was reverse-transcribed to cDNA using the Reverse Transcription Reagent Kit (Takara Bio Inc., Kusatsu). The resulting cDNA was amplified via 40 cycles of real-time PCR using SYBR Green Mix (Applied Biosystems, Waltham, MA, USA). The mRNA level of each target gene was normalized to endogenous *GAPDH* expression. The ΔΔCt method was used to evaluate relative expression levels or fold changes. The primer sequences used in our study are listed in table S2.

Hypothalamic BDNF knockdown and infusion experiment

Male mice were randomly assigned to receive AAV-shRNA(BDNF) or AAV-shRNA (scramble). Briefly, mice were anesthetized with isoflurane and secured via ear and incisor bars on a stereotaxic frame. We injected AAV vectors bilaterally into the hypothalamus according to the following coordinates: −0.8 mm posterior to the bregma, ±0.3 mm lateral to the midline, and −5.0 mm below the surface of the skull. Viruses were delivered at a rate of 0.1 μl/min by a microsyringe pump connected to a Hamilton syringe with a 33-gauge needle (Hamilton, SC, USA). After injection, the syringe was slowly removed from the brain to allow sufficient viral diffusion. For administration of recombinant BDNF protein in the hypothalamus, the osmotic pump (ALZET Model 1002; 100 μl, 0.25 μl/hour) and infusion cannula (ALZET Brain Infusion Kit 3) are incubated overnight in sterile saline at 37°C before surgery. Each pump was filled with 100 μl of sterile PBS or BDNF in PBS at a concentration of 120 ng/μl. Each mouse was anesthetized and placed in a stereotactic head frame, and the tip of the infusion catheter was stereotactically positioned into the stereotaxic coordinates described above. The cannula was then secured with bone cement, and the pump was subcutaneously placed in the animal's dorsal side.

Flow cytometry and cell sorting

Immune cells were analyzed by flow cytometry, as previously described. To prevent nonspecific binding to the Fcγ receptor, single-cell suspensions were first incubated with an anti-CD16/32 antibody. Fixable viability stain 510 (564406, BD Biosciences) and the following antibodies were used for flow cytometry: CD45-APC-Cy7 (557659, BD Biosciences), CD45-PE (553081, BD Biosciences), CD11b–fluorescein isothiocyanate (FITC; 557396, BD Biosciences), CD11b-PE-Cy7 (552850, BD Biosciences), CD11b-PE (553311, BD Biosciences), CD64-APC (558539, BD Biosciences), Ly6C-PE-Cy7 (560593, BD Biosciences), Ly6C-APC (Invitrogen, 17-5932-82),

Ly6G-APC (560599, BD Biosciences), Ly6G-FITC (551460, BD Biosciences), F4/80-BV421 (565411, BD Biosciences), CD3e-BV421(564008, BD Biosciences), CD3e-PE (12-0031-81, eBioscience), CD4-APC(553051, BD Biosciences), CD8a-PE (553033, BD Biosciences), CD8a-FITC (553031, BD Biosciences), MHCII-BV421 (743870, BD Biosciences), CCR2-PE (FAB5538P, R&D Systems), CD86-PE (553692, BD Biosciences), CD206-APC (565250, BD Biosciences), and CD31-PE (553373, BD Biosciences). Flow cytometry and cell sorting were performed using a FACSAria flow cytometer (BD Biosciences). Data are expressed as the absolute number of cells per milligram of tissue and were analyzed using the FlowJo software.

Statistical analysis

All data are expressed as means ± SEM. The GraphPad PRISM software (version 8.3.0.538; GraphPad Software, San Diego, CA, USA) was used to analyze the data and compile the results. Data normality was determined using the Shapiro-Wilk test. Unpaired Student's *t* test or nonparametric Mann-Whitney *U* test was used to compare means between groups. For multiple comparisons, one-way analysis of variance (ANOVA) followed by Bonferroni's post hoc analysis or a nonparametric Kruskal-Wallis test with Dunn's multiple comparisons test was performed. A *P* value of 0.05 or less was considered statistically significant.

SUPPLEMENTARY MATERIALS

Supplementary material for this article is available at https://science.org/doi/10.1126/sciadv.abm3436

View/request a protocol for this paper from *Bio-protocol*.

REFERENCES AND NOTES

1. J. A. Ezekowitz, P. Kaul, J. A. Bakal, P. W. Armstrong, R. C. Welsh, F. A. McAlister, Declining in-hospital mortality and increasing heart failure incidence in elderly patients with first myocardial infarction. *J. Am. Coll. Cardiol.* **53**, 13–20 (2009).
2. A. S. Zannas, M. Jia, K. Hafner, J. Baumert, T. Wiechmann, J. C. Pape, J. Arloth, M. Ködel, S. Martinelli, M. Roitman, S. Röh, A. Haehle, R. T. Emeny, S. Iurato, T. Carrillo-Roa, J. Lahti, K. Räikkönen, J. G. Eriksson, A. J. Drake, M. Waldenberger, S. Wahl, S. Kunze, S. Lucae, B. Bradley, C. Gieger, F. Hausch, A. K. Smith, K. J. Ressler, B. Müller-Myhsok, K. H. Ladwig, T. Rein, N. C. Gassen, E. B. Binder, Epigenetic upregulation of FKBP5 by aging and stress contributes to NF-κB-driven inflammation and cardiovascular risk. *Proc. Natl. Acad. Sci. U.S.A.* **116**, 11370–11379 (2019).
3. J. E. Dimsdale, Psychological stress and cardiovascular disease. *J. Am. Coll. Cardiol.* **51**, 1237–1246 (2008).
4. J. H. Milsum, A model of the eustress system for health/illness. *Behav. Sci.* **30**, 179–186 (1985).
5. L. Cao, E. Y. Choi, X. Liu, A. Martin, C. Wang, X. Xu, M. J. During, White to brown fat phenotypic switch induced by genetic and environmental activation of a hypothalamic-adipocyte axis. *Cell Metab.* **14**, 324–338 (2011).
6. Y. Song, Y. Gan, Q. Wang, Z. Meng, G. Li, Y. Shen, Y. Wu, P. Li, M. Yao, J. Gu, H. Tu, Enriching the housing environment for mice enhances their NK cell antitumor immunity via sympathetic nerve-dependent regulation of NKG2D and CCR5. *Cancer Res.* **77**, 1611–1622 (2017).
7. J. Chabry, S. Nicolas, J. Cazareth, E. Murris, A. Guyon, N. Glaichenhaus, C. Heurteaux, A. Petit-Paitel, Enriched environment decreases microglia and brain macrophages inflammatory phenotypes through adiponectin-dependent mechanisms: Relevance to depressive-like behavior. *Brain Behav. Immun.* **50**, 275–287 (2015).
8. F. Qi, Z. Zuo, J. Yang, S. Hu, Y. Yang, Q. Yuan, J. Zou, K. Guo, Z. Yao, Combined effect of BCG vaccination and enriched environment promote neurogenesis and spatial cognition via a shift in meningeal macrophage M2 polarization. *J. Neuroinflammation* **14**, 32 (2017).
9. S. Brod, T. Gobbetti, B. Gittens, M. Ono, M. Perretti, F. D'Acquisto, The impact of environmental enrichment on the murine inflammatory immune response. *JCI Insight* **2**, e90723 (2017).
10. S. Garofalo, G. D'Alessandro, G. Chece, F. Brau, L. Maggi, A. Rosa, A. Porzia, F. Mainiero, V. Esposito, C. Lauro, G. Benigni, G. Bernardini, A. Santoni, C. Limatola, Enriched environment reduces glioma growth through immune and non-immune mechanisms in mice. *Nat. Commun.* **6**, 6623 (2015).
11. T. A. Forbes, E. Z. Goldstein, J. L. Dupree, B. Jablonska, J. Scafidi, K. L. Adams, Y. Imamura, K. Hashimoto-Torii, V. Gallo, Environmental enrichment ameliorates perinatal brain injury and promotes functional white matter recovery. *Nat. Commun.* **11**, 964 (2020).
12. J. Nithianantharajah, A. J. Hannan, Enriched environments, experience-dependent plasticity and disorders of the nervous system. *Nat. Rev. Neurosci.* **7**, 697–709 (2006).
13. E. Bernberg, I. J. Andersson, L. M. Gan, A. S. Naylor, M. E. Johansson, G. Bergström, Effects of social isolation and environmental enrichment on atherosclerosis in ApoE$^{-/-}$ mice. *Stress (Amsterdam, Netherlands)* **11**, 381–389 (2008).
14. L. E. Sousa, I. F. D. Favero, F. S. Bezerra, A. B. F. Souza, A. C. Alzamora, Environmental enrichment promotes antioxidant effect in the ventrolateral medulla and kidney of renovascular hypertensive rats. *Arq. Bras. Cardiol.* **113**, 905–912 (2019).
15. D. Jia, H. Jiang, X. Weng, J. Wu, P. Bai, W. Yang, Z. Wang, K. Hu, A. Sun, J. Ge, Interleukin-35 promotes macrophage survival and improves wound healing after myocardial infarction in mice. *Circ. Res.* **124**, 1323–1336 (2019).
16. Y. Li, M. Dong, Q. Wang, S. Kumar, R. Zhang, W. Cheng, J. Xiang, G. Wang, K. Ouyang, R. Zhou, Y. Xie, Y. Lu, J. Yi, H. Duan, J. Liu, HIMF deletion ameliorates acute myocardial ischemic injury by promoting macrophage transformation to reparative subtype. *Basic Res. Cardiol.* **116**, 30 (2021).
17. U. Hofmann, S. Frantz, Role of lymphocytes in myocardial injury, healing, and remodeling after myocardial infarction. *Circ. Res.* **116**, 354–367 (2015).
18. P. M. Ridker, B. M. Everett, T. Thuren, J. G. MacFadyen, W. H. Chang, C. Ballantyne, F. Fonseca, J. Nicolau, W. Koenig, S. D. Anker, J. J. P. Kastelein, J. H. Cornel, P. Pais, D. Pella, J. Genest, R. Cifkova, A. Lorenzatti, T. Forster, Z. Kobalava, L. Vida-Simiti, M. Flather, H. Shimokawa, H. Ogawa, M. Dellborg, P. R. F. Rossi, R. P. T. Troquay, P. Libby, R. J. Glynn, Antiinflammatory therapy with canakinumab for atherosclerotic disease. *N. Engl. J. Med.* **377**, 1119–1131 (2017).
19. S. D. Prabhu, N. G. Frangogiannis, The biological basis for cardiac repair after myocardial infarction: From inflammation to fibrosis. *Circ. Res.* **119**, 91–112 (2016).
20. L. Timmers, G. Pasterkamp, V. C. de Hoog, F. Arslan, Y. Appelman, D. P. de Kleijn, The innate immune response in reperfused myocardium. *Cardiovasc. Res.* **94**, 276–283 (2012).
21. R. Xiao, S. M. Bergin, W. Huang, A. M. Slater, X. Liu, R. T. Judd, E. D. Lin, K. J. Widstrom, S. D. Scoville, J. Yu, M. A. Caligiuri, L. Cao, Environmental and genetic activation of hypothalamic BDNF modulates T-cell immunity to exert an anticancer phenotype. *Cancer Immunol. Res.* **4**, 488–497 (2016).
22. C. K. Huang, D. Dai, H. Xie, Z. Zhu, J. Hu, M. Su, M. Liu, L. Lu, W. Shen, G. Ning, J. Wang, R. Zhang, X. Yan, Lgr4 governs a pro-inflammatory program in macrophages to antagonize post-infarction cardiac repair. *Circ. Res.* **127**, 953–973 (2020).
23. X. Yan, A. Anzai, Y. Katsumata, T. Matsuhashi, K. Ito, J. Endo, T. Yamamoto, A. Takeshima, K. Shinmura, W. Shen, K. Fukuda, M. Sano, Temporal dynamics of cardiac immune cell accumulation following acute myocardial infarction. *J. Mol. Cell. Cardiol.* **62**, 24–35 (2013).
24. J. Tang, Y. Shen, G. Chen, Q. Wan, K. Wang, J. Zhang, J. Qin, G. Liu, S. Zuo, B. Tao, Y. Yu, J. Wang, M. Lazarus, Y. Yu, Activation of E-prostanoid 3 receptor in macrophages facilitates cardiac healing after myocardial infarction. *Nat. Commun.* **8**, 14656 (2017).
25. S. Epelman, K. J. Lavine, A. E. Beaudin, D. K. Sojka, J. A. Carrero, B. Calderon, T. Brija, E. L. Gautier, S. Ivanov, A. T. Satpathy, J. D. Schilling, R. Schwendener, I. Sergin, B. Razani, E. C. Forsberg, W. M. Yokoyama, E. R. Unanue, M. Colonna, G. J. Randolph, D. L. Mann, Embryonic and adult-derived resident cardiac macrophages are maintained through distinct mechanisms at steady state and during inflammation. *Immunity* **40**, 91–104 (2014).
26. S. A. Dick, J. A. Macklin, S. Nejat, A. Momen, X. Clemente-Casares, M. G. Althagafi, J. Chen, C. Kantores, S. Hosseinzadeh, L. Aronoff, A. Wong, R. Zaman, I. Barbu, R. Besla, K. J. Lavine, B. Razani, F. Ginhoux, M. Husain, M. I. Cybulsky, C. S. Robbins, S. Epelman, Self-renewing resident cardiac macrophages limit adverse remodeling following myocardial infarction. *Nat. Immunol.* **20**, 29–39 (2019).
27. G. Bajpai, C. Schneider, N. Wong, A. Bredemeyer, M. Hulsmans, M. Nahrendorf, S. Epelman, D. Kreisel, Y. Liu, A. Itoh, T. S. Shankar, C. H. Selzman, S. G. Drakos, K. J. Lavine, The human heart contains distinct macrophage subsets with divergent origins and functions. *Nat. Med.* **24**, 1234–1245 (2018).
28. L. Cao, X. Liu, E. J. Lin, C. Wang, E. Y. Choi, V. Riban, B. Lin, M. J. During, Environmental and genetic activation of a brain-adipocyte BDNF/leptin axis causes cancer remission and inhibition. *Cell* **142**, 52–64 (2010).
29. E. Castrén, L. Monteggia, Brain-derived neurotrophic factor signaling in depression and antidepressant action. *Biol. Psychiatry* **90**, 128–136 (2021).
30. S. Okada, M. Yokoyama, H. Toko, K. Tateno, J. Moriya, I. Shimizu, A. Nojima, T. Ito, Y. Yoshida, Y. Kobayashi, H. Katagiri, T. Minamino, I. Komuro, Brain-derived neurotrophic factor protects against cardiac dysfunction after myocardial infarction via a central nervous system-mediated pathway. *Arterioscler. Thromb. Vasc. Biol.* **32**, 1902–1909 (2012).
31. H. Song, F. Fang, F. K. Arnberg, D. Mataix-Cols, L. Fernandez de la Cruz, C. Almqvist, K. Fall, P. Lichtenstein, G. Thorgeirsson, U. A. Valdimarsdottir, Stress related disorders and risk of cardiovascular disease: Population based, sibling controlled cohort study. *BMJ* **365**, l1255 (2019).

32. M. F. Gonzalez Fleitas, M. L. Aranda, H. H. Dieguez, J. D. Devouassoux, M. S. Chianelli, D. Dorfman, R. E. Rosenstein, Pre-ischemic enriched environment increases retinal resilience to acute ischemic damage in adult rats. *Exp. Eye Res.* **178**, 198–211 (2019).
33. J. Y. Chen, Y. Yu, Y. Yuan, Y. J. Zhang, X. P. Fan, S. Y. Yuan, J. C. Zhang, S. L. Yao, Enriched housing promotes post-stroke functional recovery through astrocytic HMGB1-IL-6-mediated angiogenesis. *Cell Death Dis.* **3**, 17054 (2017).
34. S. R. Cho, H. Suh, J. H. Yu, H. H. Kim, J. H. Seo, C. H. Seo, Astroglial activation by an enriched environment after transplantation of mesenchymal stem cells enhances angiogenesis after hypoxic-ischemic brain injury. *Int. J. Mol. Sci.* **17**, 1550 (2016).
35. E. Bernberg, I. J. Andersson, L. M. Gan, A. S. Naylor, M. E. Johansson, G. Bergstrom, Effects of social isolation and environmental enrichment on atherosclerosis in $ApoE^{-/-}$ mice. *Stress* **11**, 381–389 (2008).
36. N. G. Frangogiannis, The inflammatory response in myocardial injury, repair, and remodelling. *Nat. Rev. Cardiol.* **11**, 255–265 (2014).
37. A. Mantovani, S. K. Biswas, M. R. Galdiero, A. Sica, M. Locati, Macrophage plasticity and polarization in tissue repair and remodelling. *J. Pathol.* **229**, 176–185 (2013).
38. P. Ramachandran, A. Pellicoro, M. A. Vernon, L. Boulter, R. L. Aucott, A. Ali, S. N. Hartland, V. K. Snowdon, A. Cappon, T. T. Gordon-Walker, M. J. Williams, D. R. Dunbar, J. R. Manning, N. van Rooijen, J. A. Fallowfield, S. J. Forbes, J. P. Iredale, Differential Ly-6C expression identifies the recruited macrophage phenotype, which orchestrates the regression of murine liver fibrosis. *Proc. Natl. Acad. Sci. U.S.A.* **109**, E3186–E3195 (2012).
39. K. Yu, Y. Wu, Q. Zhang, H. Xie, G. Liu, Z. Guo, F. Li, J. Jia, S. Kuang, R. Hu, Enriched environment induces angiogenesis and improves neural function outcomes in rat stroke model. *J. Neurol. Sci.* **347**, 275–280 (2014).
40. T. Buch, F. L. Heppner, C. Tertilt, T. J. Heinen, M. Kremer, F. T. Wunderlich, S. Jung, A. Waisman, A Cre-inducible diphtheria toxin receptor mediates cell lineage ablation after toxin administration. *Nat. Methods* **2**, 419–426 (2005).
41. C. Liu, Y. Yang, C. Chen, L. Li, J. Li, X. Wang, Q. Chu, L. Qiu, Q. Ba, X. Li, H. Wang, Environmental eustress modulates β-ARs/CCL2 axis to induce anti-tumor immunity and sensitize immunotherapy against liver cancer in mice. *Nat. Commun.* **12**, 5725 (2021).
42. M. Maroder, D. Bellavia, A. Vacca, M. P. Felli, I. Screpanti, The thymus at the crossroad of neuroimmune interactions. *Ann. N. Y. Acad. Sci.* **917**, 741–747 (2000).
43. P. C. Casarotto, M. Girych, S. M. Fred, V. Kovaleva, R. Moliner, G. Enkavi, C. Biojone, C. Cannarozzo, M. P. Sahu, K. Kaurinkoski, C. A. Brunello, A. Steinzeig, F. Winkel, S. Patil, S. Vestring, T. Serchov, C. Diniz, L. Laukkanen, I. Cardon, H. Antila, T. Rog, T. P. Piepponen, C. R. Bramham, C. Normann, S. E. Lauri, M. Saarma, I. Vattulainen, E. Castrén, Antidepressant drugs act by directly binding to TRKB neurotrophin receptors. *Cell* **184**, 1299–1313.e19 (2021).
44. T. T. Dai, B. Wang, Z. Y. Xiao, Y. You, S. W. Tian, Apelin-13 upregulates BDNF against chronic stress-induced depression-like phenotypes by ameliorating HPA axis and hippocampal glucocorticoid receptor dysfunctions. *Neuroscience* **390**, 151–159 (2018).
45. J. C. Arévalo, S. H. Wu, Neurotrophin signaling: Many exciting surprises! *Cell. Mol. Life Sci.* **63**, 1523–1537 (2006).
46. J. P. Konhilas, L. A. Leinwand, The effects of biological sex and diet on the development of heart failure. *Circulation* **116**, 2747–2759 (2007).
47. G. Bajpai, A. Bredemeyer, W. Li, K. Zaitsev, A. L. Koenig, I. Lokshina, J. Mohan, B. Ivey, H. M. Hsiao, C. Weinheimer, A. Kovacs, S. Epelman, M. Artyomov, D. Kreisel, K. J. Lavine, Tissue resident CCR2– and CCR2+ cardiac macrophages differentially orchestrate monocyte recruitment and fate specification following myocardial injury. *Circ. Res.* **124**, 263–278 (2019).
48. D. Kong, Q. Wan, J. Li, S. Zuo, G. Liu, Q. Liu, C. Wang, P. Bai, S. Z. Duan, B. Zhou, F. Gounari, A. Lyu, M. Lazarus, R. M. Breyer, Y. Yu, DP1 activation reverses age-related hypertension via NEDD4L-mediated T-bet degradation in T cells. *Circulation* **141**, 655–666 (2020).

Acknowledgments: We would like to thank C. Wang for helping with mouse colony management and the staff for assistance with animal procedures and experiments. **Funding:** This study was supported by the National Natural Science Foundation of China (82130010 to A.-J.S. and 82100274 to D.-L.J.), National Science Fund for Distinguished Young Scholars (81725002), Shanghai Sailing Program (21YF1405900), and China Postdoctoral Science Foundation (2021M690678). **Author contributions:** P.-Y.B. and A.-J.S. designed the research. P.-Y.B., S.-Q.C., D.-L.J., and L.-H.P. performed experiments. P.-Y.B., S.-Q.C., D.-L.J., L.-H.P., and A.-J.S. analyzed and discussed the results. P.-Y.B., L.-H.P., and A.-J.S. wrote the article. S.-Q.C., L.-H.P., C.-B.L., J.L., W.L., Y.Y., M.-Y.S., N.-F.W., W.-W.R., and J.-B.G. provided technical support and contributed to the discussion of the article. S.-Q.C, D.-L.J., L.-H.P., and A.-J.S. did critical editing. **Competing interests:** The authors declare that they have no competing interests. **Data and materials availability:** All data needed to evaluate the conclusions in the paper are present in the paper and/or the Supplementary Materials.

Submitted 1 October 2021
Accepted 10 March 2022
Published 27 April 2022
10.1126/sciadv.abm3436